

RESEARCH ARTICLE

A free-boundary model of a motile cell explains turning behavior

Masoud Nickaeen¹, Igor L. Novak¹, Stephanie Pulford², Aaron Rumack³, Jamie Brandon⁴, Boris M. Slepchenko¹, Alex Mogilner^{5*}

1 Richard D. Berlin Center for Cell Analysis and Modeling, Department of Cell Biology, University of Connecticut Health Center, Farmington, CT, United States of America, **2** Center for Engineering Learning & Teaching, University of Washington, Seattle, WA, United States of America, **3** Department of Computer Science, Cornell University, Ithaca, NY, United States of America, **4** Department of Mathematics, Adrian College, Adrian, MI, United States of America, **5** Courant Institute and Department of Biology, New York University, New York, NY, United States of America

* mogilner@cims.nyu.edu



OPEN ACCESS

Citation: Nickaeen M, Novak IL, Pulford S, Rumack A, Brandon J, Slepchenko BM, et al. (2017) A free-boundary model of a motile cell explains turning behavior. *PLoS Comput Biol* 13(11): e1005862. <https://doi.org/10.1371/journal.pcbi.1005862>

Editor: Martin Meier-Schellersheim, National Institutes of Health, UNITED STATES

Received: April 7, 2017

Accepted: October 31, 2017

Published: November 14, 2017

Copyright: © 2017 Nickaeen et al. This is an open access article distributed under the terms of the [Creative Commons Attribution License](https://creativecommons.org/licenses/by/4.0/), which permits unrestricted use, distribution, and reproduction in any medium, provided the original author and source are credited.

Data Availability Statement: Numerical codes used to solve the model equations are in the file RotatingCell.zip at <http://cims.nyu.edu/~mogilner/codes.html>.

Funding: This work was supported by the National Institutes of Health grants: 2 P41 RR013186-15 from the National Center for Research Resources and 9 P41 GM103313-15 and U54 GM64346 from the National Institute of General Medical Sciences. AR and JB were supported by the National Science Foundation grant DMS 1460967. AM was supported by the National Institutes of Health grant

Abstract

To understand shapes and movements of cells undergoing lamellipodial motility, we systematically explore minimal free-boundary models of actin-myosin contractility consisting of the force-balance and myosin transport equations. The models account for isotropic contraction proportional to myosin density, viscous stresses in the actin network, and constant-strength viscous-like adhesion. The contraction generates a spatially graded centripetal actin flow, which in turn reinforces the contraction via myosin redistribution and causes retraction of the lamellipodial boundary. Actin protrusion at the boundary counters the retraction, and the balance of the protrusion and retraction shapes the lamellipodium. The model analysis shows that initiation of motility critically depends on three dimensionless parameter combinations, which represent myosin-dependent contractility, a characteristic viscosity-adhesion length, and a rate of actin protrusion. When the contractility is sufficiently strong, cells break symmetry and move steadily along either straight or circular trajectories, and the motile behavior is sensitive to conditions at the cell boundary. Scanning of a model parameter space shows that the contractile mechanism of motility supports robust cell turning in conditions where short viscosity-adhesion lengths and fast protrusion cause an accumulation of myosin in a small region at the cell rear, destabilizing the axial symmetry of a moving cell.

Author summary

To understand shapes and movements of simple motile cells, we systematically explore minimal models describing a cell as a two-dimensional actin-myosin gel with a free boundary. The models account for actin-myosin contraction balanced by viscous stresses in the actin gel and uniform adhesion. The myosin contraction causes the lamellipodial boundary to retract. Actin protrusion at the boundary counters the retraction, and the balance of protrusion and retraction shapes the cell. The models reproduce a variety of motile

GM068952 and by US Army Research Office grant W911NF-17-1-0417. The funders had no role in study design, data collection and analysis, decision to publish, or preparation of the manuscript.

Competing interests: The authors have declared that no competing interests exist.

shapes observed experimentally. The analysis shows that the mechanical state of a cell depends on a small number of parameters. We find that when the contractility is sufficiently strong, cells break symmetry and move steadily along either straight or circular trajectory. Scanning model parameters shows that the contractile mechanism of motility supports robust cell turning behavior in conditions where deformable actin gel and fast protrusion destabilize the axial symmetry of a moving cell.

Introduction

Cell motility is a fundamental biological phenomenon that underlies many physiological processes in health and disease, including wound healing, embryogenesis, immune response, and metastatic spread of cancer cells [1], to name a few. Understanding the full complexity of cell motility, exacerbated by complex biochemical regulation, poses enormous challenges. One of them is multiple, sometimes redundant, sometimes complementary or even competing, mechanisms of motility [2]. Many researchers hold the view, which we share, that the way to face this challenge is to study all these mechanisms thoroughly, and then proceed with a more holistic approach.

One of the best studied types of motility is the lamellipodial motility on flat, hard and adhesive surfaces [3], in which broad and flat motile appendages—lamellipodia—spread around the cell body. Biochemical regulation plays an important role in the lamellipodial dynamics, but minimal mechanisms of the lamellipodial motility, such as growth and spreading of a flat actin network wrapped in plasma membrane and myosin-powered contraction of this network, are mechanical in nature [3]. While many cell types exhibit the lamellipodial motility, one model system, the fish epithelial keratocyte cell, contributed very prominently to the understanding of lamellipodial mechanics, due to its large lamellipodium, streamlined for rapid and steady locomotion [4, 5].

There are at least three distinct mechanical states of this system. The cells can be in a stationary symmetric state, with a ring-like lamellipodium around the cell body [6]. Spontaneously, even if slowly, the cells self-polarize, so that the lamellipodium retracts at the prospective rear and takes on a fan-like shape, upon which the cell starts crawling with a constant speed and steady shape [6, 7]. Often, cell's trajectory changes from straight to circular—the cells start turning [8].

Mechanics of keratocyte movements has been studied extensively [4, 5, 7, 9]. Two principal mechanisms enable the keratocyte motility. First, polymerization of the polarized actin network at the front pushes forward the membrane at the leading edge, stretching the membrane and creating membrane tension at the sides; the membrane then snaps at the rear and pulls forward the depolymerizing actin network [10]. Second, contractile forces generated by myosin, lagging behind in a moving cell, hold the cell sides and retract the rear, allowing the front to protrude [5]. This and stick-slip dynamics of adhesions were recently shown to generate the cell self-polarization [7].

One of the fundamental questions of cell motility concerns dynamics of the cell shape: how do the actin-myosin mechanics in the cell bulk interact with actin growth and membrane mechanics at the boundary to shape, stabilize and propel the cell? This question requires mathematical insight, and in the last two decades, keratocyte mechanics were extensively modeled mathematically. The mathematical problem arising in these models is generally challenging, given that the motile cell is a free-boundary object, in which deformations of the cell shape

depend on, and in turn affect, the actin-myosin movements and forces inside the cell. The history of the free-boundary cell modeling was recently reviewed in [11].

To reduce the mathematical complexity of the problem, one can ignore the mechanics in the lateral cross section and consider a simplified one-dimensional (1D) model, essentially representing the cell as a 1D strip of an actin-myosin gel. Mathematical models of this kind [12–15] provided valuable insight into conditions for symmetry breaking, motility initiation, and stabilization of the anterior-posterior length of the moving cell. Modeling the front-to-rear cell mechanics is not the only 1D approach: one can also disregard the bulk of the actin-myosin network and hypothesize that the essential dynamics is concentrated at the very edge of the cell; this allows one to approximate the cell shape by a 1D dynamic contour, which protrudes or retracts locally according to some set of rules. A number of such models [16–19] revealed that a small set of the boundary deformation rules can generate an unexpected variety of dynamic cell shapes mimicking a number of observed motile cell types. The first such model was a Graded Radial Extension mathematical model [20], which integrated experimental data and posited that actin polymerization at the lamellipodial boundary results in protrusion of the cell front and sides in the direction locally normal to the boundary, with spatially graded rate maximal at the center of the leading edge and decreasing towards the sides.

A more accurate mathematical rendering of the lamellipodia is achieved via a full 2D free-boundary model. Its general concept, first introduced in [21], is as follows. Actin-myosin contraction in the bulk of the 2D lamellipodium generates a centripetal actin flow that redistributes myosin powering the contraction; this feedback results in a spatially graded flow that tends to retract the lamellipodial boundary. Actin growth at the boundary results in protrusion countering the retraction, and the balance of protrusion and retraction shapes the lamellipodium, feeding back to the actin-myosin contraction in the bulk of the lamellipodium. The question is: what kind of cell shapes and movements does this model predict?

To address this question, 2D models of actin-myosin mechanics were employed to reproduce steady-state shapes and speed, as well as self-polarization, of a motile cell [5, 7, 22], but a number of important issues have not been adequately explored, including turning behavior and dependence of the motile behavior on the model parameters and boundary conditions. In this paper, we resolve these issues by simulating numerically a minimal free-boundary model described in the next section. We find that 1) cells are stationary when contractility is weak, 2) when contractility is strong, cells break symmetry and move steadily along either straight or circular trajectory, 3) cells exhibit turning behavior when fast protrusion destabilizes the axial symmetry of a planar myosin distribution or cell shape, and 4) motile behavior of a cell is sensitive to conditions of force balance at the cell boundary.

Models and methods

Mechanics plays a dominant role in keratocyte motility, while the role of biochemical regulation is less clear, and is probably of less importance [3]; thus we focus on mechanical formulation. Moreover, at least for the self-polarization phenomenon, the contractile mechanism of motility is dominant compared to the graded actin polymerization [7], and so we concentrate on the myosin generated forces and movements, and for simplicity assume that the actin growth is uniform around the cell boundary.

The model consists of force-balance and myosin transport equations,

$$\begin{aligned} \eta \Delta_{\mathbf{x}} \mathbf{U} + \sigma \nabla_{\mathbf{x}} M - \zeta \mathbf{U} &= 0 \\ \partial_t M &= \nabla_{\mathbf{x}} \cdot (D_{\text{eff}} \nabla_{\mathbf{x}} M - \mathbf{U}_{\text{eff}} M) \end{aligned} \quad (1)$$

for the velocity of actin flow $\mathbf{U}(\mathbf{X}, t)$ and myosin concentration $M(\mathbf{X}, t)$ defined locally for $\mathbf{X} \in$

$\Omega(t)$, where $\Omega(t)$ is a moving 2D domain representing cell geometry. Note, that all model equations are formulated in the lab frame of references. We discuss the validity of approximating the flat lamellipodium as a 2D domain in the thin-cell limit in the Supplemental Material. The model is similar to an actomyosin dynamic model suggested in [5, 23], and to active gel models of the soft matter physics [24]. In the force balance equation, the first term describes the force due to passive viscous stresses in the deforming actin network, where η is the effective actin viscosity. The form of this term corresponds to the viscous shear stress in the Stokes equation of hydrodynamics; we emphasize that the actin polymer mesh is compressible (fluid cytoplasm can be squeezed easily into the dorsal direction in the cell [23]), and so there is no incompressibility condition. In the Supplemental Material, we discuss the conditions under which the effects of hydrostatic pressure and Darcy flow are negligible in the lamellipodium. Because the movement of the cell takes place on the slow time scales, we do not consider viscoelastic effects [23]. Also, as was done in many modeling studies [25], we ignore for simplicity subtle and complex interplay between bulk and shear viscous stresses.

The second term in the force-balance equation describes the divergence of the myosin contractile stress. As in [5, 23, 24], we assume the stress to be isotropic and proportional to the myosin density, with σ denoting the force per unit of myosin density. The third term describes the effective viscous drag arising from creeping movement of F-actin relative to a substrate, mediated by dynamic adhesions and characterized by the viscous drag coefficient ξ . The linear dependence of this drag on actin velocity is a standard assumption made in cell mechanics models; for some cases, this assumption was verified experimentally.

The second of Eq (1) describes myosin transport. Kinetics of myosin can be interpreted in terms of transitions between two states, a state of free myosin diffusing in the cytoplasm and a state in which myosin is bound to the actin network [23]; clusters of the bound myosin both contract the actin network and move with it. For the transitions occurring on a fast time scale, the overall transport is well approximated by a diffusion-advection equation, and we assume this limit in our model here. Additional discussion of the myosin transport is in the Supplemental Material. For low viscosity and slow diffusion, however, using \mathbf{U} as an advection velocity and constant diffusion coefficients D results in singular solutions, in which M and \mathbf{U} develop Dirac-delta singularities. The effect is reminiscent of the collapsing phenomenon in a 2D version of the Keller-Segel chemotaxis model [26], which is mathematically similar to our mechanical model. The singular solutions are obviously unrealistic, given that myosin molecules have a finite size. The excluded volume effect can be taken into account by introducing effective velocities [27], $\mathbf{U}_{\text{eff}} = \mathbf{U}(1 - M/M_{\text{max},u})$, which approach zero when $M \rightarrow M_{\text{max},u}$. But in a free-boundary problem, the actual maximum of myosin concentrations may significantly exceed $M_{\text{max},u}$. This is because in motile solutions, myosin accumulates at the rear of the cell, where it is also swept forward by a moving boundary; mathematically, this effect originates from the Rankine-Hugoniot boundary condition described in the next paragraph. Thus, the effect of molecular crowding on myosin velocity should generally be written as: $\mathbf{U}_{\text{eff}} = \mathbf{U}(1 - M/M_{\text{max},u})$, if $M < M_{\text{max},u}$, and zero otherwise. Because diffusion is also affected by the crowding, the effective diffusivity in Eq (1) is $D_{\text{eff}} = D(1 - M/M_{\text{max},d})$, with a value of the cut-off $M_{\text{max},d}$ that exceeds the actual maximal densities of myosin [28]. Overall, using a tighter myosin cut-off for advection, $M_{\text{max},u} < M_{\text{max},d}$, helps avoiding the singularities and numerical instabilities associated with them in a wide range of model parameters. We also explored the possibility that the anti-crowding effects come from an attenuation of the myosin stress when the myosin density is too high, described in detail in the Supplemental Material.

One of our goals is to investigate how boundary conditions, specified in a free boundary problem at a moving cell boundary $\partial\Omega(t)$, affect the model behavior. We explore two types of conditions for the force-balance equation. One of them is the zero actin velocity at the

boundary, $\mathbf{U}|_{\partial\Omega(t)} = 0$, which assumes a very narrow band of very strong adhesions near the cell edge that rapidly adjust their positions to the instantaneous location of the boundary. Many experimental observations indicate the presence of such a band. We will term this version of the model a zero-velocity (ZV) model. Alternatively, in the absence of the sticky band, the force balance is reflected by a zero stress condition, introduced earlier in [5, 23]: $\mathbf{n} \cdot (\eta \nabla_x \mathbf{U} + M \hat{\mathbf{I}})|_{\partial\Omega(t)} = 0$, where $\hat{\mathbf{I}}$ is the unit tensor and \mathbf{n} is the outward normal. This assumes that the membrane tension is small relative to the contractile and viscous stresses. We will call this variant of the model a zero-stress (ZS) model. Both versions of the model share a no-flux Rankine-Hugoniot boundary condition for myosin, $\mathbf{n} \cdot (-D_{\text{eff}} \nabla_x M + (\mathbf{U}_{\text{eff}} - \mathbf{V}_f)M)|_{\partial\Omega(t)} = 0$, where \mathbf{V}_f is the local boundary velocity.

Kinematics of the boundary is modeled by a superposition of locally normal protrusion powered by actin growth and retraction stemming from the centripetal actin flow: $\mathbf{V}_f = V_p \mathbf{n} + \mathbf{U}|_{\partial\Omega(t)}$. The approximation of the speed of normal protrusion V_p is somewhat different in the two versions of the model, as described below.

In the ZS model, V_p is defined uniformly along the boundary but depends on the cell size: $V_p = V_0(A_0/A) - K(A - A_0(A_0/A)^n)$, where $A = |\Omega(t)|$, $A_0 = |\Omega(0)|$, and $n = 2$. The first term represents the rate of membrane displacement due to actin growth with a rate constant V_0 . The cell-size dependence of this term reflects an effective drop in actin concentration in an expanding cell, but this term alone would still produce an infinite cell expansion for large V_0 . Realistically, cell stretching is limited by membrane tension, which is represented in V_p by $-KA$ term; this is consistent with previous experiments and modeling [4, 5, 29]. The term $\propto (A_0/A)^n$ reflects cytoplasmic resistance to contractile forces and thus excludes collapsing of the cell in the model with small V_0 . Mathematically, the quadratic nonlinearity in the area dependence appears to be the lowest nonlinearity preventing the cell collapse in the ZS model. Overall, the second term in V_p , combining the effects of membrane tension and cytoplasm resistance to contraction, plays an area-preserving role (with the parameter K describing sensitivity of V_p to changes in A). Indeed, if $A < A_0$, the membrane tension decreases, whereas actin polymerization accelerates and the resistance to further contraction rapidly grows. On the other hand, if $A > A_0$, the membrane tension increases rapidly stopping the actin growth.

For the ZV model, where $\mathbf{U}|_{\partial\Omega(t)} = 0$ and $\mathbf{V}_f = V_p \mathbf{n}$, there must be a nontrivial variation of V_p along the boundary, since for a uniform V_p , the cell centroid is always stationary. Based on experimental observations and models showing that myosin can impede protrusion by bundling actin filaments at the boundary [18], we hypothesized that the actin growth rate is a decreasing function of local myosin density. Correspondingly, we use the following expression for V_p in the ZV model, $V_p = V_0(A_0/A)(1 + M|_{\partial\Omega(t)}/M_0)^{-1} - K(A - A_0)$, where M_0 is a threshold beyond which myosin inhibits actin growth almost entirely. The expression has essentially the same dependence on cell area as in the ZS model, except that for the ZV model, $n = 0$ proved to be sufficient for preserving the target area. We discuss derivation of the mathematical expression for V_p from the force balance at the lamellipodial boundary and provide additional explanations in the Supplemental Material.

Nondimensionalization

To nondimensionalize the model, we use the following set of units. The length unit L is defined as a characteristic linear size of the cell with a target area, $L = \sqrt{A_0/\pi}$ (e.g., if this cell is a circle, L is its radius). We further choose $L^2 D^{-1}$ and M_0 as the units of time and myosin concentration, respectively. Then the dimensionless variables, differential operator, and current and target cell areas are, respectively, $t = TDL^{-2}$, $\mathbf{x} = \mathbf{X}L^{-1}$, $\mathbf{u} = \mathbf{U}LD^{-1}$, $m = M/M_0$, $\nabla \equiv \nabla_x = L\nabla_x$, |

$\omega = |\Omega|L^{-2}$ and $a_0 = A_0L^{-2}$. Correspondingly, Eqs (1) takes the form,

$$\begin{aligned} \partial_t m &= \nabla \cdot (d_{\text{eff}} \nabla m - \mathbf{u}_{\text{eff}} m) \\ \alpha \Delta \mathbf{u} + \beta \nabla m - \mathbf{u} &= \mathbf{0} \end{aligned} \quad (2)$$

where $\mathbf{u}_{\text{eff}} = \mathbf{u}(1 - m/m_{\text{max},u})$, if $m < m_{\text{max},u}$, and zero otherwise, and $d_{\text{eff}} = 1 - m/m_{\text{max},d}$. Eqs (2) include two dimensionless parameters: the dimensionless viscosity-adhesion length parameter $\alpha = \eta L^{-2} \xi^{-1}$ and the myosin contractility constant $\beta = \sigma M_0 (D\xi)^{-1}$. Note that the mechanical effect of localized myosin contraction spreads on the length scale $\sqrt{\eta/\xi}$, so the viscosity-adhesion length parameter α is the ratio of the length scale of the mechanical action to the cell size. The first of Eqs (2), a diffusion-advection equation for myosin, is subject to the mass-conserving zero-flux boundary condition, $\mathbf{n} \cdot (-d_{\text{eff}} \nabla m + (\mathbf{u}_{\text{eff}} - \mathbf{v}_f) m)|_{\partial\omega(t)} = 0$, yielding an additional dimensionless parameter $\mu_{\text{tot}} = \iint_{\omega(t)} m \cdot d|\omega|$. The dimensionless boundary conditions for the force-balance equation (the second of Eqs (2)) in the ZV and ZS models are $\mathbf{u}|_{\partial\omega(t)} = 0$ and $\mathbf{n} \cdot (\alpha \nabla \mathbf{u} + \beta m \hat{\mathbf{I}})|_{\partial\omega(t)} = 0$, respectively.

The dimensionless boundary velocity equation is $\mathbf{v}_f = v_p \mathbf{n} + \mathbf{u}|_{\partial\omega(t)}$. In this equation, the dimensionless rate of membrane displacement caused by the actin polymerization and area preserving factors is $v_p = v_0 a_0 / a - k(a - a_0(a_0/a)^n)$, where $v_0 = V_0 L / D$ and $a = |\omega(t)|$. For the ZS model, $n = 2$, whereas for the ZV model, $n = 0$ and there is the additional dependence on m in the first term: $v_p = v_0 a_0 / (a(1 + m|_{\partial\omega(t)})) - k(a - a_0)$.

Note that varying parameter $k = KL^3 D^{-1}$ is equivalent to rescaling the actin polymerization constant v_0 . Also, because the myosin contractility constant β enters Eq (2) in combination with m , varying β is similar to rescaling μ_{tot} ; in fact, β could be formally excluded from the ZS model by employing a different concentration unit, and the same is true for the ZV model defined in a fixed geometry, see section *Cell becomes motile when myosin contractility is higher than critical*. We therefore focus in our study on the role played by three essentially independent model parameters: α , μ_{tot} and v_0 .

Initial conditions

Steady dynamics of a motile cell were explored by solving Eqs (2) in domains with free boundaries. Note that even though the force-balance equation does not involve time derivatives in and of itself, the coupled system (2) constitutes an initial-value problem and one must specify initial conditions for both variables and the domain, $m(\mathbf{x}, 0)$, $\mathbf{u}(\mathbf{x}, 0)$, and $\omega(0)$.

To elucidate processes leading to instability of an initially symmetric stationary state of a motile cell and its transitioning to motility, we used initial conditions based on a stationary steady state of the ZV model in a circular geometry $\omega(0) = \{(x, y): x^2 + y^2 \leq 1\}$ (such that $a_0 = |\omega(0)| = \pi$): $\mathbf{u}(\mathbf{x}, 0) = 0$, $m(\mathbf{x}, 0) = (\mu_{\text{tot}}/|\omega|)(1 - gx)$. Note the linear horizontal gradient, added to a steady-state uniform myosin distribution to probe stability of a stationary state; the gradient steepness g was assigned values from (0, 1]. Note also that given the symmetry of $\omega(0)$, the definition of $m(\mathbf{x}, 0)$ ensures that the solution has a prescribed μ_{tot} . The initial conditions specified above were used in solving both ZV and ZS models throughout this study.

Numerical methods

Numerical solutions of the ZV and ZS models were obtained using a generalized version of a mass-conservative algorithm originally developed for solving parabolic equations in moving domains with known kinematics [30]. The method has been shown to converge in space with an order close to 2 in L^2 -norm and ensures exact local mass conservation. The latter is achieved by employing finite-volume spatial discretization [31] and natural neighbor interpolation [32].

The algorithm was developed for modeling cell motility in *Virtual Cell* (VCell), a general-purpose computational framework for modeling cellular phenomena in realistic geometries [33].

To be applicable to a free-boundary problem with the models described above, the original method had to be augmented in several aspects. First, the boundary kinematics is generally not known *a priori* but rather needs to be computed on the basis of the rates that are functions of state variables—the actin velocities, in the ZS model, and the myosin concentrations, in the ZV model. To approximate values of the variables at the points of the boundary where the boundary velocities need to be evaluated, we used the second-order bilinear extrapolation. Once the boundary velocities are obtained, the cell boundary is advanced using a robust front-tracking technique implemented in FronTier, a freely available C++ library for tracking interfaces in two and three dimensions [34]. Accuracy of the algorithm coupled to FronTier was evaluated using several benchmark examples, one of which was based on the models of this study. The tests have shown that the accuracy of the original algorithm is preserved, if in addition to the second-order extrapolation, the front-tracking routine is also at least second-order accurate.

Second, the system (2), consisting of the coupled parabolic and elliptic equations, is nonlinear. Indeed, the equations are coupled via the advection term of the parabolic equation and myosin-dependent stress term in the elliptic equation, as well as through the boundary conditions at the moving boundary; also, the effective transport parameters are functions of the myosin concentration. To solve the system, we implemented a segregated solution strategy [31], in which equations are solved one at a time and nonlinear terms are treated by fixed-point iterations. One advantage of the segregated solver is that it prevents the matrix of a linearized system from becoming very large even with very fine computational grids. The system was advanced in time using an implicit backward Euler time discretization.

For each time step, the segregated method performs fixed-point iterations in two steps. First, we solve for actin velocities using fixed myosin concentrations from the previous iteration. The obtained velocities are then used as a fixed advection field at the next step, where we solve the linearized transport equation for myosin concentrations. Note that at this step, the values of the myosin concentrations in the discretized time derivative correspond to the previous time step, not to the previous fixed-point iteration. At the end of the iteration, maximum absolute differences of two consecutive iterates are checked for convergence. If they are within prescribed tolerances, the iterations stop and the solver reports the velocities and myosin concentrations as the current time step values, otherwise it proceeds to the next iteration and continues until the iterations converge or an imposed maximum for the number of iterations is exceeded. The algorithm is illustrated below for one time step by the mathematical pseudocode, where m^k and \mathbf{u}^k are the variable values at the k th time step, m_n^{k+1} and \mathbf{u}_n^{k+1} are the n th iterates for the $(k+1)$ th time step, MaxNumIters is the maximum allowed number of iterations, and $\|\cdot\|_\infty$ denotes the L^∞ -norm.

```

set  $m_1^{k+1} = m^k$  and  $\mathbf{u}_1^{k+1} = \mathbf{u}^k$ 
for  $n = 1$ : MaxNumIters
  - solve  $\alpha \Delta \mathbf{u}_{n+1}^{k+1} + \beta \nabla m_n^{k+1} - \mathbf{u}_{n+1}^{k+1} = 0$  to get  $\mathbf{u}_{n+1}^{k+1}$ 
  - evaluate  $\mathbf{u}_{\text{eff}}$  and  $d_{\text{eff}}$  using  $\mathbf{u}_{n+1}^{k+1}$  and  $m_n^{k+1}$ 
  - solve  $(m_{n+1}^{k+1} - m^k) / \Delta t = \nabla \cdot (d_{\text{eff}} \nabla m_{n+1}^{k+1} - \mathbf{u}_{\text{eff}} m_{n+1}^{k+1})$  to get  $m_{n+1}^{k+1}$ 
  - calculate absolute errors  $\|\mathbf{u}_{n+1}^{k+1} - \mathbf{u}_n^{k+1}\|_\infty$  and  $\|m_{n+1}^{k+1} - m_n^{k+1}\|_\infty$ 
  - if solution converged, break the loop, else  $m_n^{k+1} = m_{n+1}^{k+1}$ ,  $\mathbf{u}_n^{k+1} = \mathbf{u}_{n+1}^{k+1}$ 
end of segregated loop
if  $n < \text{MaxNumIters}$   $m^{k+1} = m_{n+1}^{k+1}$ ,  $\mathbf{u}^{k+1} = \mathbf{u}_{n+1}^{k+1}$ , else iterations are stagnant.

```

The segregated solver was validated against a coupled nonlinear solver implemented in COMSOL Multiphysics [35]. Good agreement was observed, with relative differences below 0.3%.

The computations were performed with the following solution parameters: the mesh sizes h varied between 0.05 and 0.16, whereas the time step was $\Delta t = ch$ with c varying from 0.0002 to 0.025 (fast-moving cells required smaller mesh sizes and time steps), the tolerance for the differences of consecutive iterates was $1E-10$, and the maximum allowed number of iterations, set at 35, was never reached.

Results

The ZV and ZS models were used to simulate transitions of a motile cell from stationary to motile state. For this, as described in section *Initial conditions*, an initially radially symmetric cell was perturbed by superimposing a linear gradient over a uniform distribution of myosin. The emerged steady states fall into three asymptotically stable mechanical modes. For some parameter values, the cell, after a finite displacement, comes to a stop, with a final radially symmetric shape and myosin distribution, indicating the stability of the stationary state (Fig 1A). For other parameters, the cell irreversibly breaks symmetry, both in terms of its shape, distribution of myosin, and actin velocity field, and either acquires unidirectional motility (Fig 1B) or locks in a rotational mode (Fig 1C).

To analyze conditions for transitioning to different types of motility, we scanned the actin growth constant (v_0) and the contractility parameter (μ_{tot}) for two values of viscosity-adhesion length parameter, $\alpha = 0.5$ and $\alpha = 1$. The values of other model parameters, $\beta = 5$, $a_0 = \pi$, $k = 1.5$, $m_{\text{max},u} = 15$ and $m_{\text{max},d} = 125$, were fixed in all simulations; the choice of these values ensures that the corresponding section of parameter space is representative of various states. The results of parameter scanning are presented in Fig 2 showing cell mechanical states as functions of the model parameters.

It should be noted that distinguishing between translational and rotational modes is sometimes ambiguous, particularly for the states near the borders between the corresponding regions in the parameters space. For example, some states of the ZS model shown in the diagrams of Fig 2 as translating were in fact only ‘piecewise unidirectional’, as the cell in those states would on occasion change its direction. Moreover, in some states in the ZS model, identified as translations, also neighboring the rotations in the diagrams of Fig 2, the cell actually changes its direction but very gradually, so the state could be a rotation with a very long radius. As a practical rule, we labeled states as rotations only if the radius of rotation of the cell centroid was comparable to, or less than, the linear size of the cell.

Below we discuss in detail the conditions required for the straight and rotational motility in our models and the underlying mechanisms.

Cell becomes motile when myosin contractility is higher than critical

The results in Fig 2 show that cells break symmetry and transition to motility when parameter μ_{tot} exceeds a threshold. The threshold behavior originates from a positive feedback between the actin flow and myosin gradients: the contractile forces, generating the centripetal flow of myosin, are proportional to the myosin gradients, which, in turn, are reinforced by the advection of myosin. This positive feedback results in steep myosin gradients and, potentially, symmetry breaking, but below a critical value of μ_{tot} these gradients are prevented by dissipative viscous forces and myosin diffusion, and the cell remains stationary and radially symmetric. Above the critical value of μ_{tot} , steep gradients of myosin are developed and the radially symmetric stationary state becomes unstable. While kinematics of a free boundary plays a key role

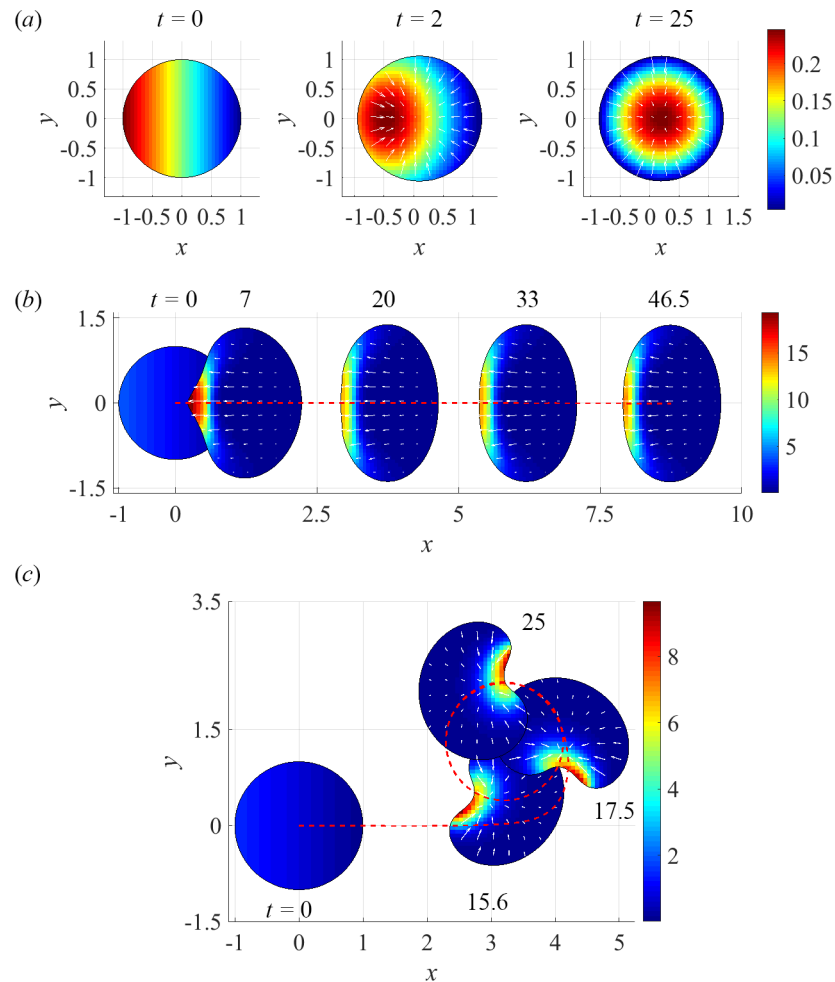


Fig 1. Asymptotically stable mechanical states (in all cases, $\alpha = 0.5$): (a) a stationary state of ZS model, $(v_0, \mu_{tot}) = (2.5, 0.125\pi)$; (b) unidirectional translation in ZV model, $(v_0, \mu_{tot}) = (2.5, 2\pi)$; (c) rotations in ZS model, $(v_0, \mu_{tot}) = (2.5, 0.75\pi)$. Pseudo-colors depict distributions of myosin; arrows are actin velocities; a red dashed line/curve shows the trajectory of a centroid.

<https://doi.org/10.1371/journal.pcbi.1005862.g001>

in the symmetry breaking and transitioning to motility in both models, the loss of symmetry in the ZV model also occurs in fixed domains. In the next section, we discuss effects of the boundary conditions for actin flow on solutions in domains with fixed and free boundaries.

Linear stability analysis can be used to estimate critical values of μ_{tot} in a simplified ZV model in a fixed domain. Consider a 1D ZV model on the fixed-length segment $\partial\omega = \{x \in (0,1)\}$ in the limit $m_{max,1}, m_{max,2} \rightarrow \infty$, so that $d_{eff} = 1$ and $u_{eff} = u(x,t)$. Then, Eqs (2) become $\alpha u_{xx} + \beta m_x - u = 0$, $m_t = m_{xx} - (um)_x$. In this model, varying the contractility constant β is equivalent to rescaling μ_{tot} . Indeed, β could be excluded altogether by renormalizing m : $\tilde{m} = \beta m$, but in what follows parameter β is kept for generality. The symmetric steady state is characterized by uniform myosin distribution and absence of actin flow, $u = 0$, $m = \mu_{tot}$. Its stability is probed by imposing small perturbations, $\delta u(x,t) = \delta u_0 \exp(\lambda t + i q x)$, $\delta m(x,t) = \delta m_0 \exp(\lambda t + i q x)$ with $0 < \delta u_0 \ll 1$, $0 < \delta m_0 \ll 1$ and $q = \pi, 2\pi, \dots$, so that $u = \delta u$ and $m = \mu_{tot} + \delta m$. The perturbations satisfy the linearized system of differential equations, $\alpha \delta u_{xx} + \beta \delta m_x - \delta u = 0$, $\delta m_t = \delta m_{xx} - \mu_{tot} (\delta u)_x$ and the corresponding system of linear algebraic equations, $-(1 + \alpha q^2) \delta u_0 + i q \beta \delta m_0 = 0$, $i q \mu_{tot} \delta u_0 + (\lambda + q^2) \delta m_0 = 0$, yields nontrivial solutions for δu_0 and δm_0 , if $\lambda(q) = q^2 (\beta \mu_{tot} (1 + \alpha q^2)^{-1} - 1)$. The

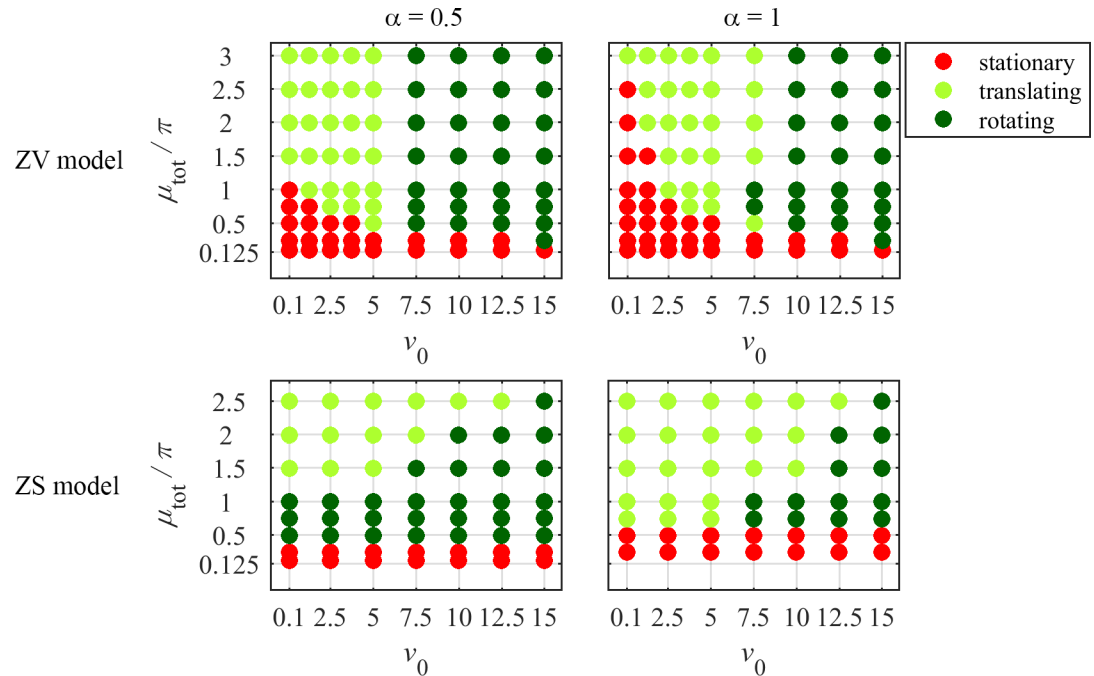


Fig 2. Mechanical states of ZV and ZS models for varying sets (v_0, μ_{tot}) and $\alpha = 0.5$ and 1 .

<https://doi.org/10.1371/journal.pcbi.1005862.g002>

perturbations grow if $\lambda(q) > 0$, with the fastest growing mode having the minimal wave number, $q_{min} = \pi$, and thus involving a large-scale redistribution of myosin. Thus, the symmetric state becomes unstable if $\beta\mu_{tot} > 1 + \pi^2\alpha$ or, in the dimensional form, $\sigma M_0 \pi L^2 > D(\xi L^2 + \pi^2 \eta)$.

The instability criterion predicts that the critical value of $\beta\mu_{tot}$ is an increasing function of α . The results of Fig 2 indicate that this prediction, while obtained by analyzing a ZV model in a fixed domain, holds for the free-boundary models as well. Indeed, the competition between the myosin contractile stress and dissipative processes, mathematically expressed in the instability condition, drives the initiation of motility in the free-boundary models. As described at the beginning of this section, the transition to motility occurs when the contractility, reinforced by the model positive feedback, prevails over the dissipation. For $\alpha \geq 1$, the dimensional form of the instability criterion reduces to $\sigma M_0 L^2 > \pi D \eta$: the total myosin stress needs to overcome the smoothing effects of actin viscosity and myosin diffusion, while the adhesion strength does not matter. In the limit of large values of α , the actin network is effectively stiff and thus does not allow for significant actin flows, which makes the cell more symmetric and as a consequence less motile and slower. Our simulations confirm this prediction (Fig 3A and 3B). In the opposite limit of highly deformable actin network, $\alpha \ll 1$, the instability criterion reduces to $\sigma M_0 > \xi D$, so the cell becomes motile if the characteristic myosin stress is able to generate actin flow that overcomes myosin diffusion, which requires the weakening of adhesions and strengthening of myosin, in agreement with the experiment [7].

Finally, it is worth noting that whereas the motility threshold in the ZS model is independent of v_0 , the critical values of μ_{tot} in the ZV model, where the actin growth is affected by myosin, vary with v_0 (Fig 2). Indeed, the cell described by the ZV model with $v_0 = 0$ would not transition to motility for any μ_{tot} because in this case, the myosin influence on the boundary is lost. Therefore, in this version of the model motility initiates only for finite values of v_0 , which drop with the increase of μ_{tot} . In the ZS model, the cell with a sufficiently high μ_{tot} initiates

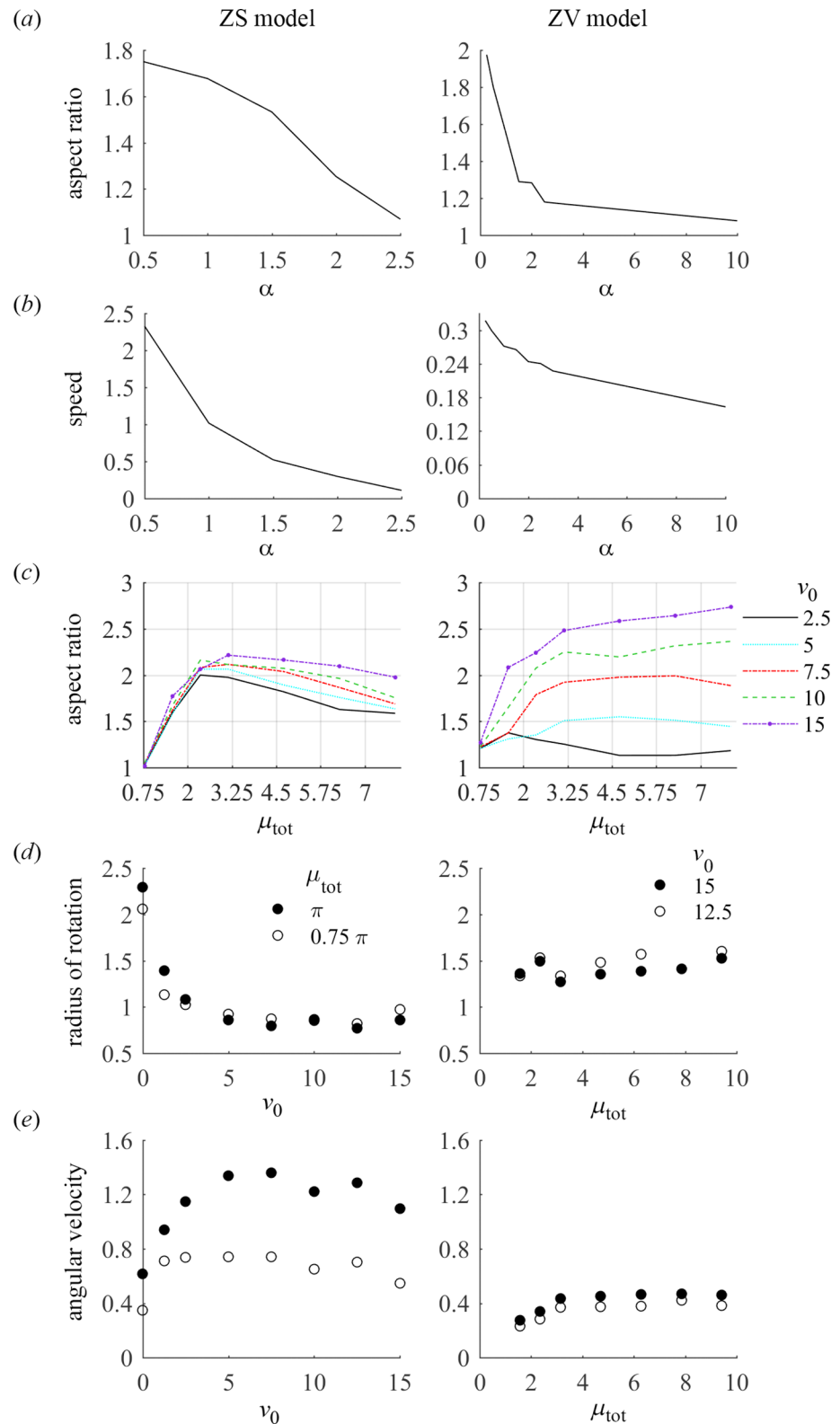


Fig 3. Aspect ratios and translational or linear rotational speeds of steadily moving cells. (a) Aspect ratio as a function of viscosity-adhesion length α ; the results were obtained with $(v_0, \mu_{tot}) = (2.5, 1.5\pi)$ for ZS model, and with $(v_0, \mu_{tot}) = (5, 1.5\pi)$ for ZV model; aspect ratios were computed as ratios of the longest to shortest distances between cell boundary and cell centroid. (b) Dimensionless translational or linear rotational

speed of a cell centroid as a function of viscosity-adhesion length α ; model parameters are as in panel (a). (c) Aspect ratio as a function of v_0 and μ_{tot} ; the results were obtained with $\alpha = 1$ for ZV model and with $\alpha = 0.5$ for ZS model. (d) Radius of rotation of a cell centroid as a function of v_0 and μ_{tot} , with values of α as in (c). (e) Dimensionless angular velocity of a cell centroid as a function of v_0 and μ_{tot} , with values of α as in (c).

<https://doi.org/10.1371/journal.pcbi.1005862.g003>

motility even as $v_0 \rightarrow 0$, because the asymmetric myosin pulls the boundary inward asymmetrically, and the area-preserving term causes the effective protrusion.

Shape and speed of the motile cell

Similar to the 1D ZV model analyzed in the previous section, the symmetric state of the 2D version of the ZV model becomes unstable for sufficiently high μ_{tot} even in a fixed geometry, with myosin relocating to the cell boundary. Fig 4A illustrates the instability of the radially symmetric steady state, in which the maximum of myosin was slightly shifted to the left of the cell center. Qualitatively, because of the zero actin velocities at the boundary, a second, initially small, local maximum of myosin appears at the boundary point closest the main maximum due to slightly faster diffusion. The competition between the two maxima lowers the myosin gradients on the left side of the main one, resulting in a net force acting on it in the left direction. Hence, the relocation of myosin to the left segment of the boundary. In the cell with a free boundary, the redistribution of myosin is conferred to boundary velocity, resulting in slower outward and eventually inward movements of the part of the boundary that becomes the cell rear. The cell movement further skews the myosin towards the rear. For the small to moderate rate of actin growth and cell speeds, the cell maintains a convex shape and a steady unidirectional motion, with myosin forming a wide band at the rear edge (Fig 1B and S1 Movie).

In the ZS model of a fixed symmetric cell, an inward actin flow at the membrane prevents myosin from accumulating there. As a result, the symmetric solution with a myosin maximum at the center remains stable even for μ_{tot} above the threshold. Indeed, shifting the maximum

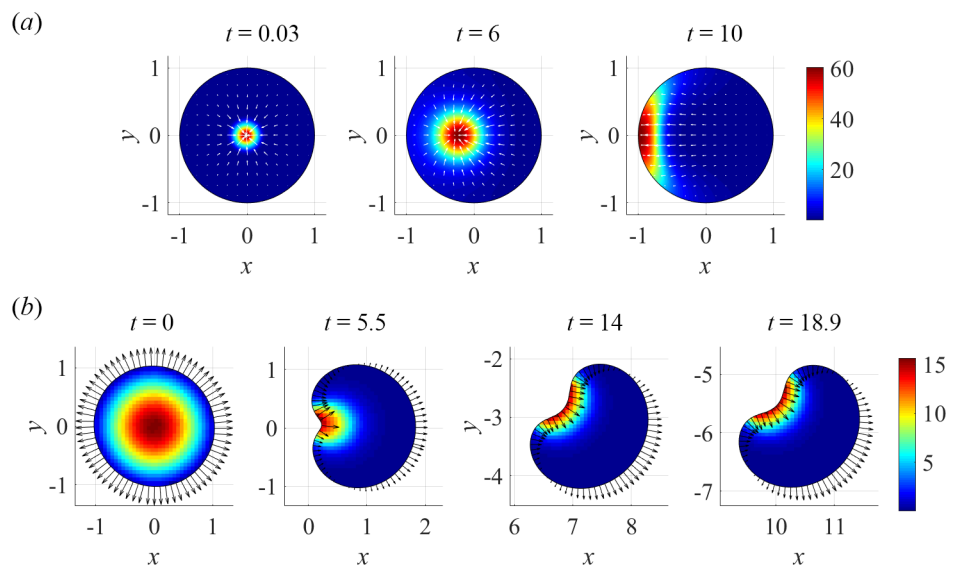


Fig 4. Symmetry breaking in a fixed circle and in a free-boundary problem. (a) Instability of a symmetric steady state of ZV model in a fixed circle: snapshots of dimensionless myosin density (pseudo-color) and actin velocities (arrows) at specified times t after myosin was slightly shifted left of center; computations were done for $\mu_{\text{tot}} = 1.5\pi$ and $\alpha = 0.5$. (b) Transition to unidirectional motility in ZS model; dimensionless myosin concentration (pseudo-colors) and boundary velocities (arrows) are shown for the solution obtained with $\alpha = 1$, $v_0 = 5$, and $\mu_{\text{tot}} = 1.5\pi$; the cell assumes steady unidirectional motility after $t = 14$ (S2 Movie).

<https://doi.org/10.1371/journal.pcbi.1005862.g004>

from the center in this case increases the myosin gradients and centripetal forces on the ‘shorter’ side and decreases them on the ‘longer’ side, netting a stabilizing force. In the free-boundary problem, however, the symmetric solution, stable at low μ_{tot} (Fig 1A), becomes unstable above the motility threshold. Fig 4B and S2 Movie illustrate a transition to unidirectional motility that occurs in the ZS model with sufficiently large μ_{tot} and small to moderate v_0 . As the myosin cluster shifts slightly from the cell center, the closer side is pulled inward faster and becomes the prospective cell rear, while the opposite side, where the protrusions are faster than retractions, becomes the cell front. In the ensued motility, myosin is pressed against the rear and in turn exerts a stronger inward force on the proximal portion of the boundary, developing a local concavity. If the movement is sufficiently fast, the myosin spreads along the portion of the boundary with negative curvature. This positive feedback between the myosin asymmetry, actin flow, and cell movement is the key to the stable motility.

Our simulations show that the aspect ratio of a steadily moving cell varies between 1 and 3 (Fig 3C), in agreement with experimental observations [5]. Note that in contrast to the ZV model, where the cell aspect ratio grows moderately with v_0 , it becomes essentially independent of model parameters in the ZS model with $\mu_{\text{tot}}/\pi > 1$. This can be qualitatively understood by noting that myosin, which in a moving cell accumulates in the middle of the rear, exerts comparable forces on the front and side portions of the boundary. Then, because the myosin-generated flow decreases with distance at similar rates in all directions, the distances from the rear to the front and the sides should be on the same order, yielding the average aspect ratio ~ 2 .

The ZS model generally predicts significantly higher cell speeds compared to those in the ZV model (Fig 5A). This is because in the ZS model, the fast centripetal flows generated by myosin at the rear boundary tend to decrease the cell area, leading to fast effective protrusion at the front, as actin can grow rapidly against the lowered membrane tension. As a result, the cell speed increases but the cell area decreases with total myosin (Fig 5B). Interestingly, the cell speed in the ZS model decreases slightly with the actin growth rate v_0 , which can be understood by noting that the cell area in this model increases with v_0 , thus mitigating the effect of myosin. In the ZV model, the cell speed is virtually insensitive to μ_{tot} for $\mu_{\text{tot}} > \pi$, because the term with v_0 in the expression for v_p becomes inessential for $m \sim \mu_{\text{tot}}/\pi > 1$. For the same reason, the cell area is also insensitive to μ_{tot} .

Importantly, our model predicts that there are no short-wavelength instabilities in the cell shape (like fingering instabilities characteristic for some physical free-boundary models), which is supported by the experiment: there are small fluctuations on the experimentally observed cell boundaries, but they mostly do not grow.

Mechanics of the straight and turning motility

The most nontrivial and important property of our models is that they predict rotational states with a radius of rotation comparable to the cell size in large regions of their parameter space (Fig 2). Note that both the radius of rotation and the angular velocity are not particularly sensitive to parameter values (Fig 3D and 3E).

Emergence of cell turning in the models can be qualitatively understood by analyzing the loss of stability of a planar axial symmetry characteristic of the straight moving cell. In the ZV model, the steady rotations are observed for v_0 exceeding a threshold that is largely insensitive to either α or μ_{tot} . Fig 6 and S3 Movie illustrate, for a particular parameter set, how rotations come about in the ZV model during a transient movement following a ‘nudge’ applied to a stationary cell in the form of an initial horizontal gradient of myosin. The initial convex cell shape is favorable for maintaining a unipolar axially symmetric myosin distribution, and the

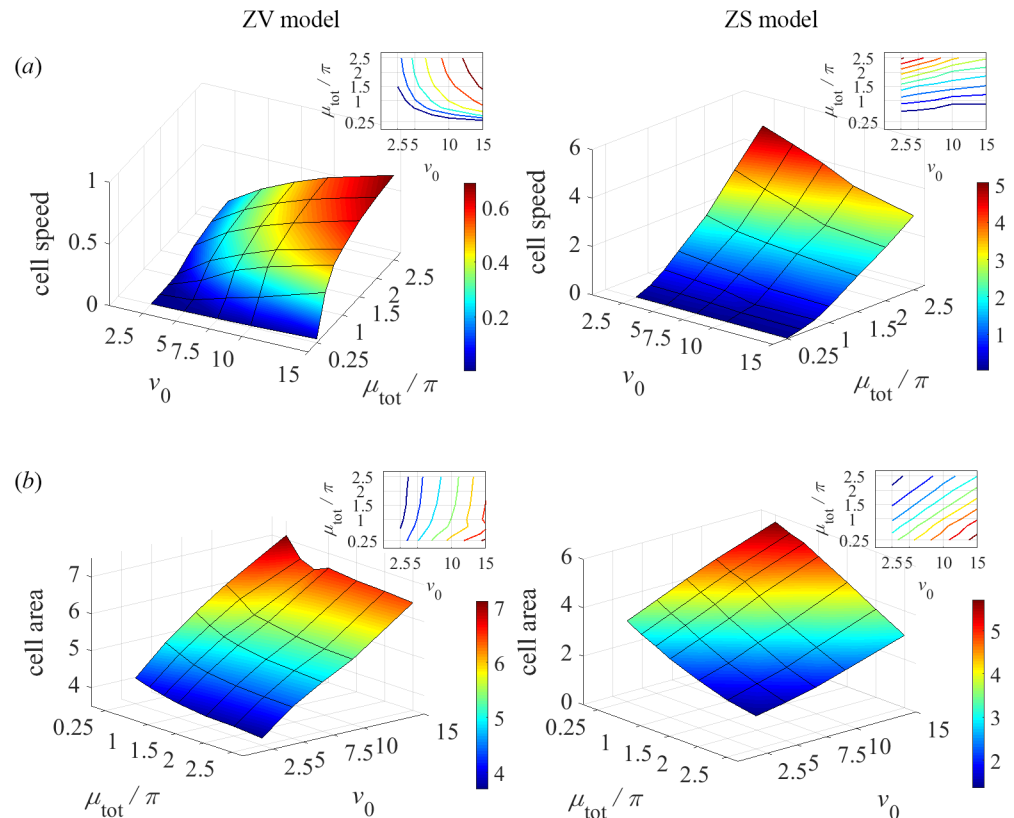


Fig 5. Cell speeds and areas as functions of v_0 and μ_{tot} . (a) Dimensionless translational or linear rotational speed of a cell centroid were obtained with $\alpha = 1$ for ZV model and $\alpha = 0.5$ for ZS model. (b) Dimensionless steady-state areas for values of α as in panel (a). Insets in both panels: corresponding level sets.

<https://doi.org/10.1371/journal.pcbi.1005862.g005>

resulting motility is unidirectional. But due to sufficiently large v_0 , fast boundary velocities at cell's sides tend to elongate the cell in y -direction, making it prone to developing a concavity at the cell rear. In such a shape, the myosin spreads along the rear part of the boundary more uniformly (Fig 6B, $t = 5$), a distribution that is no longer stable. Indeed, even a slight asymmetry in the distribution of myosin, reinforced by the positive feedback from actin velocities and myosin accumulation due to faster movement of the corresponding portion of the rear boundary, breaks the axial symmetry (Fig 6B, $t = 15$). As a result, a stable asymmetric cell shape emerges as the cell locks in rotations (Fig 6A), with myosin aggregated at a high-curvature portion of the boundary.

While the same mechanisms underlie the turning behavior in the ZS model, the two models yield significantly different results for the parameter regions of rotations. This is due to the differences in boundary conditions that reflect the opposing assumptions about the strength of adhesions at the cell periphery, and in ways of conferring the myosin dynamics onto kinematics of the boundary. Unlike the ZV model, the v_0 threshold for rotations in the ZS model strongly depends on μ_{tot} and α (Fig 2). In particular, the rotational states may exist for any v_0 , if α is sufficiently small. Note also, that the concavity of the cell shape does not always destabilize unidirectional motility in the ZS model (Fig 4B).

Fig 7 and S4 Movie illustrate the onset of turning in ZS model. If the contractility due to myosin is strong, myosin forms a radially symmetric aggregate, which in a translating cell is skewed to the cell rear, pulling the rear boundary inward and maintaining the cell propulsion.

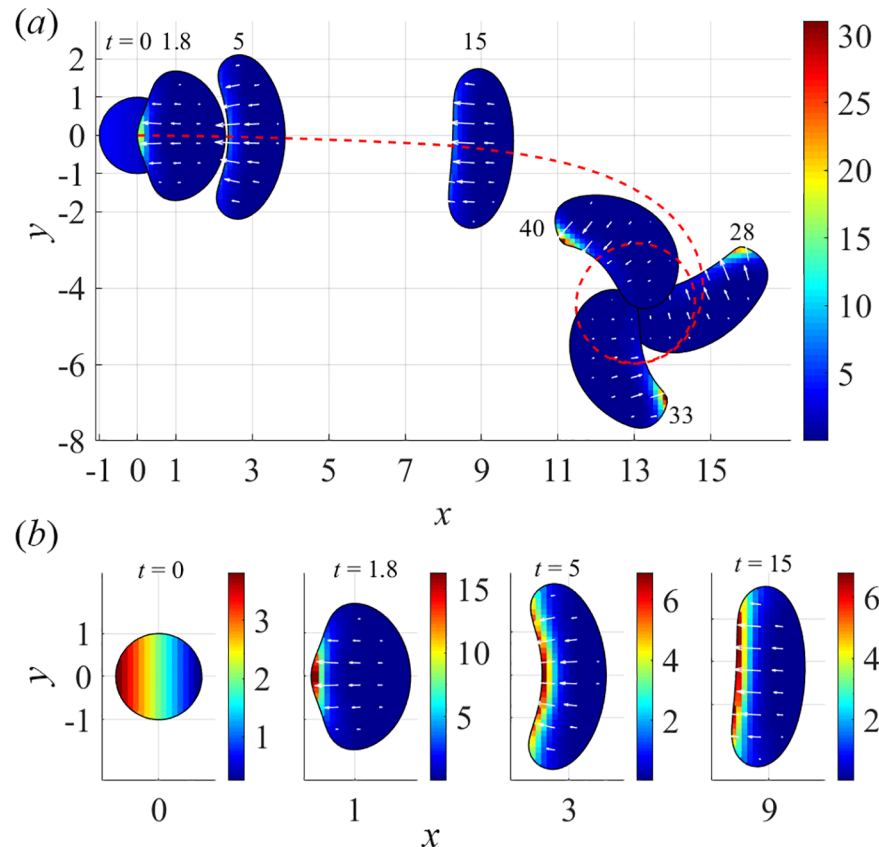


Fig 6. Onset of steady rotations in ZV model, $(v_0, \mu_{tot}, \alpha) = (12.5, 2\pi, 1)$. (a) Entire cell trajectory and cell centroid track (red dashed curve). (b) Snapshots of transient myosin distributions with individual color scales during a transient, and with white arrows representing actin velocities (S3 Movie).

<https://doi.org/10.1371/journal.pcbi.1005862.g006>

When the myosin aggregate is sufficiently close to the rear boundary, it pulls the center of the cell rear inward stronger than the sides of the rear edge, creating a ‘dip’ at the center of the rear edge and giving the cell a characteristic keratocyte fan-like shape, in which the sides of the cell lag behind the center. For the parameters in the upper left corner of the parameter space (Fig 2), the cell motion is fast, and in the frame of the cell, myosin is effectively swept towards the rear and ‘pressed’ against the rear boundary; in these conditions, the translational motility remains stable (Fig 4B). For intermediate values of μ_{tot} , the cell moves slower and the myosin aggregate maintains its radial symmetry and remains close to the cell centroid (Fig 7A, $t = 7$). In this position, myosin is able to pull inward not only the rear but also the front of the cell, making the axial symmetry of the system unstable. Indeed, even a slight random asymmetry in either the myosin distribution or the cell shape induces and reinforces the asymmetry of the other. If, for example, the myosin aggregate becomes slightly closer to one side, this side is pulled inward faster than the other, which brings even more myosin to the side that is pulled inward, because the shift of that side effectively sweeps myosin towards it (Fig 7A, $t = 9$).

Once the axial symmetry of cell shape and the position of the myosin aggregate is broken (Fig 7A, $t = 23.5$), the boundary velocity field becomes asymmetric as well (Fig 7B). It is then clear that a steady movement of a cell with an asymmetric shape and asymmetric boundary velocities (where faster displacements occur at the location of higher myosin gradients) must involve rotations. Indeed, by connecting consecutively the ends of the arrows representing normal displacements of points of the boundary in Fig 7B, one recovers the same contour in a

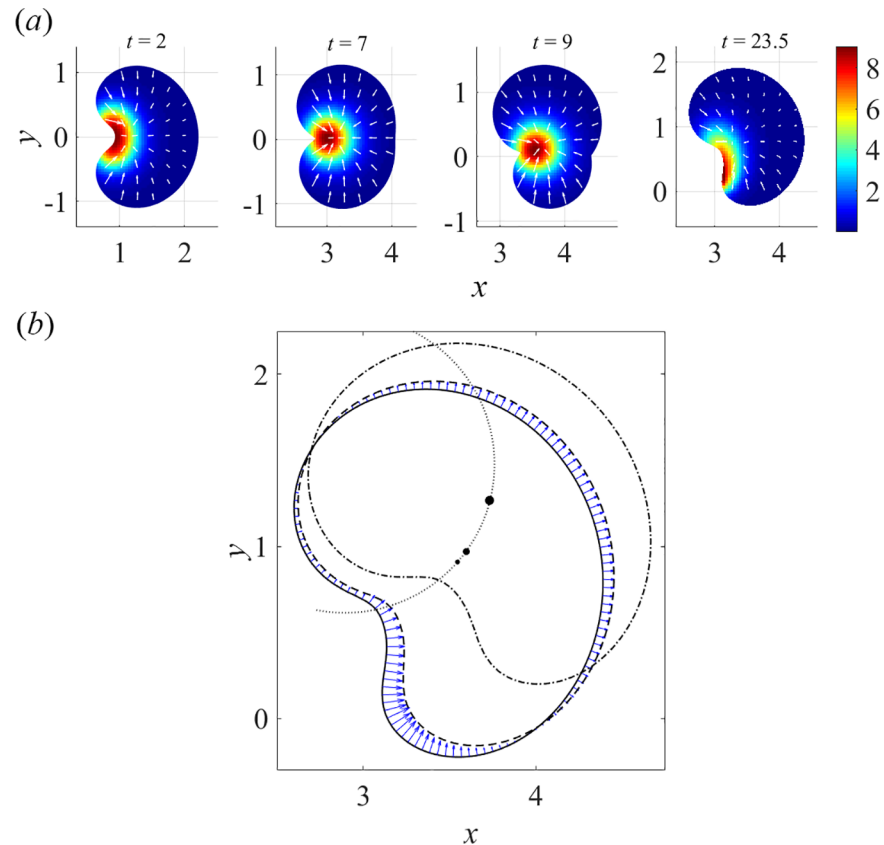


Fig 7. Steady rotations in ZS model, $(v_0, \mu_{tot}, \alpha) = (2.5, 0.75\pi, 0.5)$ (see also S4 Movie). (a) Transient distributions of myosin (pseudo-colors) and actin velocities (arrows): $t = 2$, an initially symmetric cell with centroid at $(x, y) = (0, 0)$ self-polarizes and assumes fast unidirectional motility, myosin accumulates in a semi-circular band, pulling the rear inwards to form a 'dip'; $t = 7$, the cell slows down and becomes unstable, as myosin is now close enough to cell front to be able to pull it in as well; $t = 9$, loss of axial symmetry, as the lower part of the cell with steeper myosin gradients is pulled inwards faster than the upper one; $t = 23.5$: emergence of stable asymmetric myosin distribution and cell shape, as the cell locks in rotations (see Fig 1C). (b) Cell shape and boundary velocities in steady rotations. Positions of the cell boundary and centroid at $t = 23.5, 23.6$, and 24 (solid, dashed, and dotted-dashed contours, respectively, and filled circles with larger size corresponding to later time). Faster boundary velocities (arrows) in the high curvature region, consistent with the location of steep myosin gradients (panel (a)), ensure rotational motility with a circular trajectory of the centroid (dotted arc), see also Fig 1C.

<https://doi.org/10.1371/journal.pcbi.1005862.g007>

rotated position, as the centroids of the cell in different positions belong to the same circle (Fig 7B). We also note that the shape of the expanding portion of the cell boundary is reminiscent of spirals described by more abstract models of rotating free boundaries [36].

Discussion

In this paper we systematically explored the ability of a minimal actin-myosin contractility model [7, 14] to reproduce observed mechanical states of the simplest motile cell. The model analysis has shown that the mechanical state of the cell critically depends on just three dimensionless parameters representing the myosin contractility, characteristic viscosity-adhesion length, and actin growth. For the large viscosity-adhesion length, the actin network becomes effectively stiff and does not allow for significant actin flows, which makes the cell more symmetric and as a consequence less motile and slower, and in the limit of very large values of viscosity-adhesion lengths, the cell is stationary. In the opposite limit of short viscosity-adhesion

lengths, myosin forms a very small high-density aggregate, which affects the actin network only locally. In this regime, the steady motility is impossible, and the cell starts to pivot. Thus, an important conclusion is that to move straight and steadily, the cell has to keep the viscosity-adhesion length on the order of unity (to adjust the ratio of actin viscosity to adhesion strength so that it is on the order of the cell area). Interestingly, this conclusion is consistent with estimates based on the experimental data for keratocytes [5].

Intuitively, if myosin contractility is weak, the myosin spreads uniformly and the cell remains stationary and symmetric. Above a contractility threshold, the cells become motile. The mode of motility depends on the boundary conditions. For the zero actin velocity at the boundary and the sufficiently small actin growth constant and cell speed, the convex-shaped cell maintains unidirectional motility, with myosin concentrated in a band at the rear edge. With the rate of actin growth above a certain threshold, the increase of the cell speed is sufficient for the cell to lose its planar axial symmetry and start rotating. With the zero-stress boundary conditions, rotations occur for intermediate contractility strengths, whereas in the high contractility range, the fast cells stabilize their unidirectional movement, as myosin being effectively compressed into a long band at the rear edge. We found that both explored boundary conditions explain general features of the keratocyte motility, but there are interesting differences in the predicted behaviors, as discussed above.

The main finding of our study is that the contractile mechanism of motility results in a very robust turning behavior of the cell: in the models with both explored boundary conditions, the cell moving along a circular trajectory is not an anomaly but rather a solution that exists in a large region of the model parameter space. Broadly speaking, the cell starts turning in conditions of breaking the planar axial symmetry of its myosin distribution; in the ZV model the transition to rotation is controlled by the rate of actin growth, whereas in the ZS model—by all three independent model parameters. Turning motile behavior is an important part of the cell mechanical response in chemotaxis [37] and galvanotaxis [38], and our model generates intuition about the turning mechanism.

One important test of our model is that the solutions exhibit a characteristic fan-like keratocyte shape, with the side-to-side distance greater than the front-to-rear distance and aspect ratio between 1 and 3, in excellent agreement with the observations [5]. Moreover, the predicted aspect ratio in the ZS version is nontrivial and biphasic, reaching a maximum at intermediate myosin contractility and decreasing at very weak or strong contractility, indeed observed in [5]. Similarly, the model predicts that the lamellipodial area increases at higher adhesion and lower myosin contractility, and that the cell speed increases with myosin contractility, as observed [5]. Lastly, in agreement with the experiment [7], higher myosin contractility and/or lower adhesion strength are predicted to promote the cell polarization and motility initiation. One significant prediction of our model is that both self-polarization of the cell and its turning behavior can, in principle, occur, without complex adhesion dynamics. While it was observed that a nonlinear stick-slip adhesion behavior accompanied cell polarization [7], it remains an open question whether this nonlinear behavior is essential.

The model predicts that the stable motile behavior of the cell requires tight regulation of the total lamellipodial area. We hypothesized that this regulation is mechanical, through the membrane tension. Indeed, perturbations of the total membrane area and membrane tension were found to change the lamellipodial area in a predictable way, and drastic perturbations destabilized the cell [29]. We find that cell polarization may not depend on the cell ability to move: in the ZV model, myosin distribution and actin flow become asymmetric even in the stationary symmetric domain. However, for the motility initiation, protrusion of the boundary is obviously essential (note that while motility in the ZS free-boundary model with sufficiently high μ_{tot} can be initiated even with $v_0 \rightarrow 0$, the area-preserving term of V_p in this limit effectively

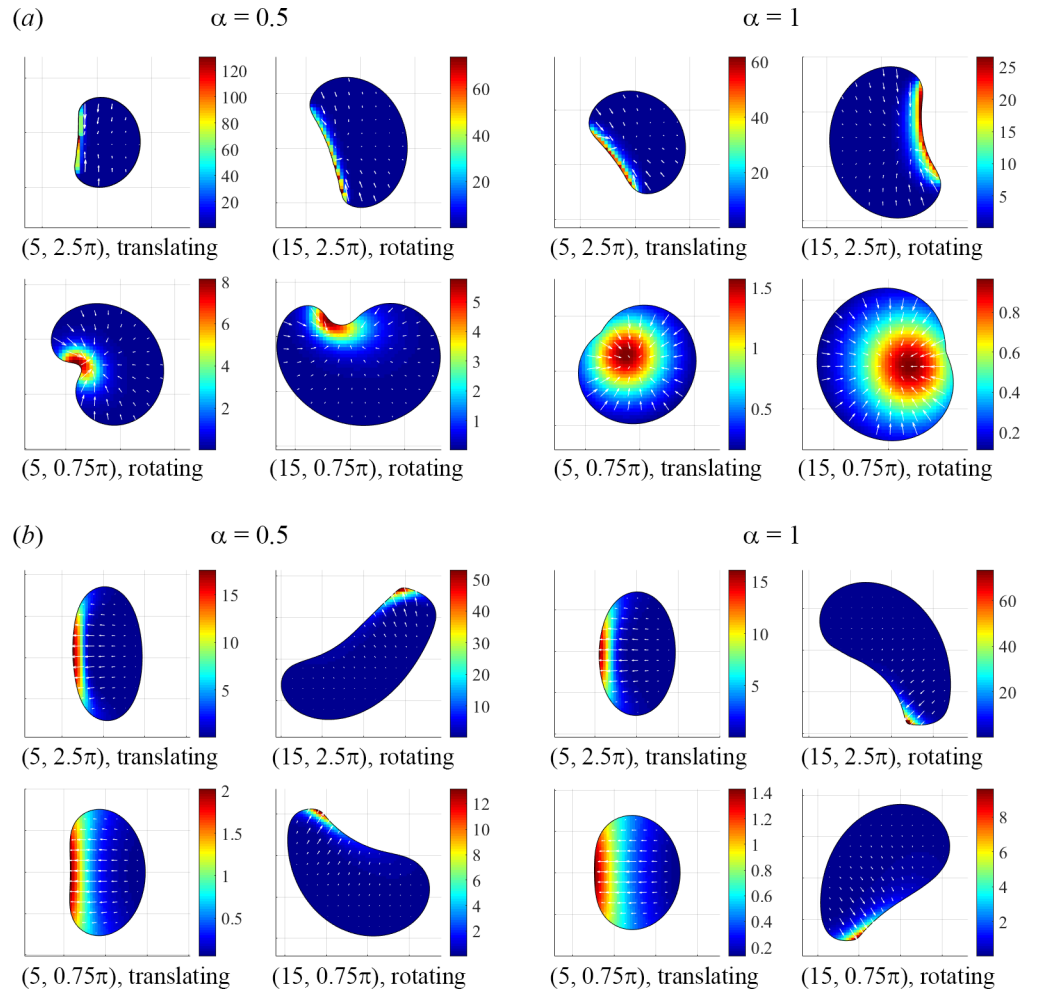


Fig 8. Steady-state cell shapes, myosin distributions (pseudo-colors), actin velocities (arrows), and motility types from solutions of the ZS (a) and ZV (b) models obtained for specified parameter values (v_0, μ_{tot}). Gridlines are spaced uniformly with $h = 1$.

<https://doi.org/10.1371/journal.pcbi.1005862.g008>

induces protrusion of the front, which is less affected by myosin, see sections *Model* and *Cell becomes motile when myosin contractility is higher than critical*).

Keratocyte motility and especially the peculiar and steady shape of the moving cell inspired a great deal of free-boundary modeling in the past decade. Our model is based on the well-justified assumption that the mechanical force balance determines cell shape and movements. Conceptually, our model is similar to the active gel models [24, 39], originating in the soft-matter physics. Some models were based on the viable idea that certain self-organized chemical patterns are upstream from the actin-myosin machinery [22, 40, 41], but majority of studies explored mechanical models [42–44]. A variety of numerical techniques—Potts models [40, 45], phase-field method [42, 44], immersed boundary method [43]—were used in respective simulations. Keratocyte polarization was modeled in [7, 46]. Alternative turning mechanisms, very different from the one predicted by our model, were computationally explored in [47, 48]. The fact that the majority of the models reproduce the keratocyte shapes and motile behavior corroborates the existing biological intuition about the keratocyte lamellipodium as the most basic, streamlined and robust actin-myosin motile structure [49]. Each of the cited studies

added invaluable insights to understanding multifaceted aspects of cell motility; a relative advantage of our model is in that it is most easily connected to the experimentally observed biophysics of force balance and myosin transport in keratocytes [5, 7].

The minimal model we explored already predicts a wealth of motile behaviors (Fig 8). It is known, however, that even the cell as streamlined for locomotion as keratocyte has complexities that far exceed our minimal model. The two main aspects that need to be added to the model to make it more realistic are: spatially graded actin polymerization independent of myosin [10] and dynamic nonlinear adhesions. Complex effects of dynamic and non-homogeneous adhesions already attracted special attention and were simulated in [7, 46, 50]. It will also be interesting to explore how the predicted cell dynamics depend on actin density [51], more complex constitutive relations for the actin-myosin stress [52], membrane curvature [53, 54], elastic [55] and anisotropic [49] effects in the actin network. Our minimal free-boundary model might be useful for future modeling of other modes of cell motility [56] and collective cell movements [57, 58]. Lastly, for decades, research focused on understanding cell movements on flat 2D surfaces, and only recently exploration of cell crawling through three-dimensional (3D) matrices, more physiologically relevant, has begun experimentally [59] and theoretically [60–62]. Extension of our model to 3D will be a challenging, yet necessary, effort.

Supporting information

S1 Appendix. Variations of the model. Supplemental text explaining effects of various model assumptions, equations and boundary conditions, including explicit consideration of actin dynamics and more detailed model of myosin transport.

(DOCX)

S1 Movie. Example of steadily moving cell predicted by simulations of the zero velocity model.

(AVI)

S2 Movie. Example of steadily moving cell predicted by simulations of the zero stress model.

(AVI)

S3 Movie. Example of rotating cell predicted by simulations of the zero velocity model.

(AVI)

S4 Movie. Example of rotating cell predicted by simulations of the zero stress model.

(AVI)

Acknowledgments

M.N., I.L.N. and B.M.S. thank Leslie Loew for his continuing support and helpful discussions.

Author Contributions

Conceptualization: Boris M. Slepchenko, Alex Mogilner.

Formal analysis: Masoud Nickaeen, Igor L. Novak, Boris M. Slepchenko, Alex Mogilner.

Investigation: Stephanie Pulford, Aaron Rumack, Jamie Brandon, Boris M. Slepchenko, Alex Mogilner.

Methodology: Alex Mogilner.

Software: Masoud Nickaeen, Igor L. Novak, Boris M. Slepchenko.

Supervision: Boris M. Slepchenko, Alex Mogilner.

Validation: Masoud Nickaeen, Igor L. Novak.

Writing – original draft: Masoud Nickaeen, Boris M. Slepchenko, Alex Mogilner.

Writing – review & editing: Masoud Nickaeen, Boris M. Slepchenko, Alex Mogilner.

References

- Ridley AJ, Schwartz MA, Burridge K, Firtel RA, Ginsberg MH, Borisy G, et al. Cell migration: integrating signals from front to back. *Science* 2003 Dec 5; 302(5651):1704–9. <https://doi.org/10.1126/science.1092053> PMID: 14657486
- Lämmermann T, Sixt M. Mechanical modes of 'amoeboid' cell migration. *Curr Opin Cell Biol.* 2009 Oct; 21(5):636–44. <https://doi.org/10.1016/j.ceb.2009.05.003> PMID: 19523798
- Verkhovskiy AB. The mechanisms of spatial and temporal patterning of cell-edge dynamics. *Curr Opin Cell Biol.* 2015 Oct; 36: 113–21. <https://doi.org/10.1016/j.ceb.2015.09.001> PMID: 26432504
- Keren K, Pincus Z, Allen GM, Barnhart EL, Marriot G, Mogilner A, et al. Mechanism of shape determination in motile cells. *Nature* 2008 May 22; 453(7194):475–80. <https://doi.org/10.1038/nature06952> PMID: 18497816
- Barnhart EL, Lee KC, Keren K, Mogilner A, Theriot JA. An adhesion-dependent switch between mechanisms that determine motile cell shape. *PLoS Biol.* 2011 May; 9(5): e1001059. <https://doi.org/10.1371/journal.pbio.1001059> PMID: 21559321
- Yam PT, Wilson CA, Ji L, Hebert B, Barnhart EL, Dye NA, et al. Actin-myosin network reorganization breaks symmetry at the cell rear to spontaneously initiate polarized cell motility. *J Cell Biol.* 2007 Sep 24; 178(7):1207–21. <https://doi.org/10.1083/jcb.200706012> PMID: 17893245
- Barnhart EL, Lee KC, Allen GM, Theriot JA, Mogilner A. Balance between cell-substrate adhesion and myosin contraction determines the frequency of motility initiation in fish keratocytes. *Proc Natl Acad Sci USA* 2015 Apr 21; 112(16):5045–50. <https://doi.org/10.1073/pnas.1417257112> PMID: 25848042
- Ream RA, Theriot JA, Somero GN. Influences of thermal acclimation and acute temperature change on the motility of epithelial wound-healing cells (keratocytes) of tropical, temperate and Antarctic fish. *J Exp Biol.* 2003 Dec; 206(24):4539–51.
- Verkhovskiy AB, Svitkina TM, Borisy GG. Network contraction model for cell translocation and retrograde flow. *Biochem Soc Symp.* 1999; 65: 207–22. PMID: 10320940
- Ofer N, Mogilner A, Keren K. Actin disassembly clock determines shape and speed of lamellipodial fragments. *Proc Natl Acad Sci USA* 2011 Dec 20; 108(51):20394–9. <https://doi.org/10.1073/pnas.1105333108> PMID: 22159033
- Holmes WR, Edelstein-Keshet L. A comparison of computational models for eukaryotic cell shape and motility. *PLoS Comput Biol.* 2012; 8(12): e1002793. <https://doi.org/10.1371/journal.pcbi.1002793> PMID: 23300403
- Gracheva M, Othmer H. A continuum model of motility in amoeboid cells. *Bull Math Biol* 2004; 66: 167–193. <https://doi.org/10.1016/j.bulm.2003.08.007> PMID: 14670535
- Carlsson AE. Mechanisms of Cell Propulsion by Active Stresses. *New J Phys.* 2011;13–073009.
- Recho P, Putelat T, Truskinovsky L. Contraction-driven cell motility. *Phys Rev Lett.* 2013 Sep 6; 111(10):108102. <https://doi.org/10.1103/PhysRevLett.111.108102> PMID: 25166712
- Kimpton LS, Whiteley JP, Waters SL, King JR, Oliver JM. Multiple travelling-wave solutions in a minimal model for cell motility. *Math Med Biol.* 2013; 30(3):241–72. <https://doi.org/10.1093/imammb/dqs023> PMID: 22789545
- Satulovsky J, Lui R, Wang YL. Exploring the control circuit of cell migration by mathematical modeling. *Biophys J.* 2008 May 1; 94(9):3671–83. <https://doi.org/10.1529/biophysj.107.117002> PMID: 18199677
- Hecht I, Skoge M, Charest P, Ben-Jacob E, Firtel R, Loomis WF, et al. Activated membrane patches guide chemotactic cell motility. *PLoS Comput Biol* 2011; 7: e1002044. <https://doi.org/10.1371/journal.pcbi.1002044> PMID: 21738453
- Lomakin AJ, Lee KC, Han SJ, Bui DA, Davidson M, Mogilner A, et al. Competition for actin between two distinct F-actin networks defines a bistable switch for cell polarization. *Nat Cell Biol.* 2015 Nov; 17(11):1435–45. <https://doi.org/10.1038/ncb3246> PMID: 26414403

19. Raynaud F, Ambühl ME, Gabella C, Bornert A, Sbalzarini IF, Meister JJ, et al. Minimal model for spontaneous cell polarization and edge activity in oscillating, rotating and migrating cells. *Nature Physics* 2016 January; 12: 367–373.
20. Lee J, Ishihara A, Theriot JA, Jacobson K. Principles of locomotion for simple-shaped cells. *Nature*. 1993 Mar 11; 362(6416):167–71. <https://doi.org/10.1038/362167a0> PMID: 8450887
21. Rubinstein B, Jacobson K, Mogilner A. Multiscale two-dimensional modeling of a motile simple-shaped cell. *Multiscale Model Sim* 2005; 3:413–439.
22. Wolgemuth CW, Stajic J, Mogilner A. Redundant mechanisms for stable cell locomotion revealed by minimal models. *Biophys J* 2011; 101: 545–553. <https://doi.org/10.1016/j.bpj.2011.06.032> PMID: 21806922
23. Rubinstein B, Fournier MF, Jacobson K, Verkhovsky AB, Mogilner A. Actin-Myosin Viscoelastic Flow in the Keratocyte Lamellipod, *Biophys J*. 2009 Oct 7; 97(7):1853–1863. <https://doi.org/10.1016/j.bpj.2009.07.020> PMID: 19804715
24. Bois JS, Jülicher F, Grill SW. Pattern formation in active fluids. *Phys Rev Lett*. 2011 Jan 14; 106(2):028103. <https://doi.org/10.1103/PhysRevLett.106.028103> PMID: 21405254
25. Foster PJ, Fürthauer S, Shelley MJ, Needleman DJ. Active contraction of microtubule networks. *eLife*. 2015 Dec 23; 4: e10837. <https://doi.org/10.7554/eLife.10837> PMID: 26701905
26. Keller EF, Segel LA. Model for chemotaxis. *J. Theor. Biol.* 1971; 30:225–234. PMID: 4926701
27. Leduc C, Padberg-Gehle K, Varga V, Helbing D, Diez S, Howard J. Molecular crowding creates traffic jams of kinesin motors on microtubules. *Proc Natl Acad Sci USA* 2012 109(16):6100–6105. <https://doi.org/10.1073/pnas.1107281109> PMID: 22431622
28. Bruggeman DAG. Calculation of various physical constants in heterogeneous substances. I. Dielectric constants and conductivity of composites from isotropic substances. *Annalen der Physik* 1935 24:636–664.
29. Lieber AD, Yehudai-Resheff S, Barnhart EL, Theriot JA, Keren K. Membrane tension in rapidly moving cells is determined by cytoskeletal forces. *Curr Biol*. 2013 Aug 5; 23(15):1409–17. <https://doi.org/10.1016/j.cub.2013.05.063> PMID: 23831292
30. Novak IL, Slepchenko BM. Conservative algorithm for parabolic problems in domains with moving boundaries. *J Comput Phys*. 2014 Mar 20; 270:203–13. <https://doi.org/10.1016/j.jcp.2014.03.014> PMID: 25067852
31. Ferziger JH, Peric M. *Computational Methods for Fluid Dynamics*, 3rd ed. Springer; 2002.
32. Sibson R., A brief description of natural neighbor interpolation. In: Barnett V, editor. *Interpreting Multivariate Data*. Chichester: John Wiley & Sons; 1981. pp. 21–36.
33. Slepchenko BM, and LM Loew. Use of Virtual Cell in studies of cellular dynamics. *Int. Rev. Cell Mol. Biol.* 2010; 283:1–56.
34. Du J, Fix B, Glimm J, Jia X, Li X, Li Y, et al. A simple package for front tracking. *J. Comput. Phys.* 2006; 213:613–628.
35. COMSOL Multiphysics. Version 5.2 [software]. Stockholm, Sweden: COMSOL AB; 2015. Available from: www.comsol.com.
36. Altschuler DJ, Altschuler SJ, Angenent SB, Wu LF. The zoo of solitons for curve shortening. *Nonlinearity* 2013; 26:1189–1226.
37. Yang HW, Collins SR, Meyer T. Locally excitable Cdc42 signals steer cells during chemotaxis. *Nat Cell Biol*. 2016 Feb; 18(2):191–201. <https://doi.org/10.1038/ncb3292> PMID: 26689677
38. Allen GM, Mogilner A, Theriot JA. Electrophoresis of cellular membrane components creates the directional cue guiding keratocyte galvanotaxis. *Curr Biol*. 2013 Apr 8; 23(7): 560–8. <https://doi.org/10.1016/j.cub.2013.02.047> PMID: 23541731
39. Tjhung E, Marenduzzo D, Cates ME. Spontaneous symmetry breaking in active droplets provides a generic route to motility. *Proc Natl Acad Sci USA* 2012 Jul 31; 109(31):12381–6. <https://doi.org/10.1073/pnas.1200843109> PMID: 22797894
40. Mareé AF, Jilkine A, Dawes A, Grieneisen VA, Edelstein-Keshet L. Polarization and movement of keratocytes: a multiscale modelling approach. *Bull Math Biol* 2006; 68(5):1169–1211. <https://doi.org/10.1007/s11538-006-9131-7> PMID: 16794915
41. MacDonald G, Mackenzie JA, Nolan M, Insall RH. A computational method for the coupled solution of reaction-diffusion equations on evolving domains and manifolds: Application to a model of cell migration and chemotaxis. *J Comput Phys*. 2016 Mar 15; 309: 207–226. <https://doi.org/10.1016/j.jcp.2015.12.038> PMID: 27330221
42. Shao D, Rappel WJ, Levine H. Computational model for cell morphodynamics. *Phys Rev Lett* 2010; 105: 108104. <https://doi.org/10.1103/PhysRevLett.105.108104> PMID: 20867552

43. Vanderlei B, Feng J, Edelstein-Keshet L. A computational model of cell polarization and motility coupling mechanics and biochemistry. *Multiscale Model Simul* 2011; 9: 1420–1443. <https://doi.org/10.1137/100815335> PMID: 22904684
44. Ziebert F, Swaminathan S, Aranson IS. Model for self-polarization and motility of keratocyte fragments. *J R Soc Interface* 2012 May 7; 9(70):1084–92. <https://doi.org/10.1098/rsif.2011.0433> PMID: 22012972
45. Nishimura SI, Sasai M. Modulation of the reaction rate of regulating protein induces large morphological and motional change of amoebic cell. *J Theor Biol.* 2007 Mar 21; 245(2):230–7. <https://doi.org/10.1016/j.jtbi.2006.09.027> PMID: 17113108
46. Ziebert F, Aranson IS. Effects of adhesion dynamics and substrate compliance on the shape and motility of crawling cells. *PLoS One* 2013 May 31; 8(5): e64511. <https://doi.org/10.1371/journal.pone.0064511> PMID: 23741334
47. Mogilner A, Rubinstein B. Actin disassembly 'clock' and membrane tension determine cell shape and turning: a mathematical model. *J Phys Condens Matter.* 2010 May 19; 22(19):194118. <https://doi.org/10.1088/0953-8984/22/19/194118> PMID: 20559462
48. Camley BA, Zhao Y, Li B, Levine H, Rappel WJ. Crawling and turning in a minimal reaction-diffusion cell motility model: coupling cell shape and Biochemistry. *Phys. Rev. E* 2017; 95: 012401. <https://doi.org/10.1103/PhysRevE.95.012401> PMID: 28208438
49. Rafelski SM, Theriot JA. Crawling toward a unified model of cell mobility: spatial and temporal regulation of actin dynamics. *Annu Rev Biochem.* 2004; 73: 209–39. <https://doi.org/10.1146/annurev.biochem.73.011303.073844> PMID: 15189141
50. Shao D, Levine H, Rappel W. Coupling actin flow, adhesion, and morphology in a computational cell motility model. *Proc Natl Acad Sci USA* 2012; 109: 6851–6856. <https://doi.org/10.1073/pnas.1203252109> PMID: 22493219
51. Kuusela E, Alt W. Continuum model of cell adhesion and migration. *J Math Biol.* 2009 Jan; 58(1–2):135–61. <https://doi.org/10.1007/s00285-008-0179-x> PMID: 18488227
52. Linsmeier I, Banerjee S, Oakes PW, Jung W, Kim T, Murrell MP. Disordered actomyosin networks are sufficient to produce cooperative and telescopic contractility. *Nat Commun.* 2016 Aug 25; 7: 12615. <https://doi.org/10.1038/ncomms12615> PMID: 27558758
53. Kabaso D, Shlomovitz R, Schloen K, Stradal T, Gov N. Theoretical model for cellular shapes driven by protrusive and adhesive forces. *PLoS Comput Biol* 2011; 7: e1001127. <https://doi.org/10.1371/journal.pcbi.1001127> PMID: 21573201
54. Du X, Doubrovinski K, Osterfield M. Self-organized cell motility from motor-filament interactions. *Biophys J.* 2012 Apr 18; 102(8):1738–45. <https://doi.org/10.1016/j.bpj.2012.03.052> PMID: 22768929
55. Zemel A, Safran SA. Active self-polarization of contractile cells in asymmetrically shaped domains. *Phys Rev E Stat Nonlin Soft Matter Phys.* 2007 Aug; 76(2 Pt 1):021905.
56. Strychalski W, Guy RD. Intracellular Pressure Dynamics in Blebbing Cells. *Biophys J.* 2016 Mar 8; 110(5):1168–79. <https://doi.org/10.1016/j.bpj.2016.01.012> PMID: 26958893
57. Camley BA, Zhang Y, Zhao Y, Li B, Ben-Jacob E, Levine H, et al. Polarity mechanisms such as contact inhibition of locomotion regulate persistent rotational motion of mammalian cells on micropatterns. *Proc Natl Acad Sci USA* 2014 Oct 14; 111(41):14770–5. <https://doi.org/10.1073/pnas.1414498111> PMID: 25258412
58. Löber J, Ziebert F, Aranson IS. Collisions of deformable cells lead to collective migration. *Sci Rep.* 2015 Mar 17; 5: 9172. <https://doi.org/10.1038/srep09172> PMID: 25779619
59. Petrie RJ, Yamada KM. Multiple mechanisms of 3D migration: the origins of plasticity. *Curr Opin Cell Biol.* 2016 Oct; 42: 7–12. <https://doi.org/10.1016/j.ceb.2016.03.025> PMID: 27082869
60. Herant M, Dembo M. Form and function in cell motility: from fibroblasts to keratocytes. *Biophys J* 2010; 98: 1408–1417. <https://doi.org/10.1016/j.bpj.2009.12.4303> PMID: 20409459
61. Tjhung E, Tiribocchi A, Marenduzzo D, Cates ME. A minimal physical model captures the shapes of crawling cells. *Nat Commun.* 2015 Jan 21; 6: 5420. <https://doi.org/10.1038/ncomms6420> PMID: 25607536
62. Zhu J, Mogilner A. Comparison of cell migration mechanical strategies in three-dimensional matrices: a computational study. *Interface Focus.* 2016 Oct 6; 6(5):20160040. <https://doi.org/10.1098/rsfs.2016.0040> PMID: 27708764

S1 Appendix: variations of the model.

2D character of the model and cytosolic pressure.

The most natural way to investigate the role of pressure in mechanics model of cell motility is to start with inclusion of mechanics of cytosol into the model. Most of research was done by using the so-called two-phase poroviscous theory of the cytoplasm, which treats the cytoskeleton and cytosol as two interpenetrative viscous fluids (Drew and Segel, 1971; Dembo and Harlow, 1986; Kuusela and Alt, 2009; Cogan and Guy, 2010). Our formulation here is close to that of (Oliver et al., 2005), but note that a number of constitutive relations and assumptions that we use are original. Characteristic poroviscous theory consists of the mass conservation equations for the network and for the cytosol:

$$\underbrace{\frac{\partial \Phi}{\partial T} + \nabla \cdot (\Phi \mathbf{U}_n)}_{\text{rate of change of network volume fraction}} = \underbrace{-J}_{\text{net rate of assembly/disassembly}}, \quad \underbrace{\frac{\partial (1-\Phi)}{\partial T} + \nabla \cdot ((1-\Phi) \mathbf{U}_s)}_{\text{rate of change of cytosol volume fraction}} = \underbrace{+J}_{\text{net rate of assembly/disassembly}}, \quad J = r(\Phi - \Phi_0), \quad (\text{Eq S1})$$

and of the force balance equations for the network,

$$\underbrace{+\eta \nabla^2 \mathbf{U}_n}_{\text{gel viscosity}} + \underbrace{\sigma \nabla M}_{\text{myosin contractile stress}} - \underbrace{\Phi \nabla P}_{\text{pressure}} = \underbrace{K(\mathbf{U}_n - \mathbf{U}_s)}_{\text{network-cytosol drag}} + \underbrace{\xi \mathbf{U}_n}_{\text{adhesion drag}}, \quad (\text{Eq S2})$$

and for the cytosol,

$$\underbrace{(1-\Phi) \nabla P}_{\text{pressure}} = \underbrace{K(\mathbf{U}_n - \mathbf{U}_s)}_{\text{network-cytosol drag}}. \quad (\text{Eq S3})$$

We also add the transport equation for myosin:

$$\frac{\partial M}{\partial T} = \underbrace{D \nabla^2 M}_{\text{myosin diffusion}} - \underbrace{\nabla \cdot (\mathbf{U}_n M)}_{\text{myosin drift with actin flow}}. \quad (\text{Eq S4})$$

Here the model dependent variables are as follows: $\mathbf{U}_n = (U_n, V_n, W_n)$, $\mathbf{U}_s = (U_s, V_s, W_s)$ are the velocities of the cytoskeletal network and cytosol, respectively; Φ is the network volume fraction; P is the cytosol's pressure; M is the myosin density. The independent variables are time T and spatial coordinate $\mathbf{X} = (X, Y, Z)$. Note that we formulate the theory in 3D. The model parameters include r , the rate of actin turnover; Φ_0 , the equilibrium volume fraction of the network; η , the network viscosity; σ , the myosin strength; K , the hydraulic resistance (network-solution drag) coefficient; ξ , the network-surface drag coefficient; D , the effective myosin diffusion coefficient. For simplicity, we neglect the so-called solvation and swelling pressures, which in principle can be equal to zero (Oliver et al., 2005). Note that all these parameters can be functions of Φ , as well as functions of \mathbf{X} and T .

The cell geometry is described by the ventral surface at $Z = 0$ and dorsal surface at $Z = H(X, Y, T)$. Boundary conditions include zero flux conditions at both boundaries for the mass conservation equations. Kinematic conditions are: at the ventral surface ($Z = 0$):

$W_n = W_s = 0$; at the dorsal surface ($Z = H(X, Y, T)$): $\mathbf{U}_n \cdot \mathbf{n} = \mathbf{U}_s \cdot \mathbf{n}$, where \mathbf{n} is the outward unit

normal vector. There are slip conditions for tangential component of all velocities at both ventral and dorsal surfaces. Finally, there is the force balance condition at the dorsal surface:

$$-(1-\Phi)P\mathbf{n} + \Phi\eta\nabla\mathbf{U}_n \cdot \mathbf{n} = \gamma\kappa\mathbf{n}. \quad (\text{Eq S5})$$

Here γ is the constant isotropic membrane tension, and κ is twice the mean curvature; $\kappa < 0$ if the dorsal surface is convex. We also assume that there is no myosin near the dorsal surface.

In addition to the model assumptions described in the main text concerning the forms of the network viscous stress, myosin contractile stress and simplified myosin transport equations, and to the standard assumptions of the two-phase poroviscous theory (Oliver et al., 2005; Cogan and Guy 2010), the main assumptions that are behind system of equations (S1)-(S5) are as follows. We assumed that the connection points between the adhesive molecular chains and actin filaments are distributed uniformly inside the 3D cell volume. We neglected possibility of more complex conditions for the network and cytosol flow at the plasma membrane that could be something between slip and stick conditions. These additional assumptions could be relaxed without changing main results in the thin-cell limit, for example, we could in principle use Navier slip law at the ventral boundary instead of the uniform adhesion drag in the 3D volume, but we wish to avoid more complex derivations.

The model (Eqs S1-5) can be scaled and non-dimensionalized as follows. We normalize Φ by 1; for consistency we use the notation $\Phi = \varphi$, $M = \bar{M}m$, where \bar{M} is the average myosin concentration. We use the thin cell approximation justified below (for the case of a high membrane tension): the average height of the cell is much smaller than the length and width of the lamellipodium, $H \sim \varepsilon L$, where L is the characteristic length/width, and $\varepsilon \ll 1$. We rescale the spatial coordinates as follows: $X = Lx, Y = Ly, Z = \varepsilon Lz, H = \varepsilon Lh$. The scale of velocity can be estimated from balancing the viscous and myosin contraction terms in (Eq S2): $U = \sigma\bar{M}L / \eta$. Thus, $U_i = Uu_i, V_i = UV_i, W_i = \varepsilon U w_i, i = n, s$. Time can be rescaled as: $T = (L/U)t = (\eta / \sigma\bar{M})t$. The scale of pressure can be estimated from balancing the pressure and Darcy terms in (Eq S3): $\bar{P} = KLU = \sigma K\bar{M}L^2 / \eta$, and $P = \bar{P}p$.

When the cell height changes slowly in the x-y plane ($\partial h / \partial x, \partial h / \partial y \ll 1$), the z-components of the network and cytosol flow velocities can be neglected in the zeroth order approximation with respect to ε : $w_n = w_s = 0$. After introducing notations $\nabla_{\perp} = (\partial / \partial x, \partial / \partial y, 0)$, $\mathbf{u}_i = (u_i, v_i, 0)$, $i = n, s$ equations (Eqs S1-5) in the zeroth order approximation with respect to ε take the following form:

$$\frac{\partial \varphi}{\partial t} + \nabla_{\perp} \cdot (\varphi \mathbf{u}_n) = \left(\frac{r\eta}{\sigma\bar{M}} \right) (\varphi_0 - \varphi), \quad \frac{\partial(1-\varphi)}{\partial t} + \nabla_{\perp} \cdot ((1-\varphi)\mathbf{u}_s) = - \left(\frac{r\eta}{\sigma\bar{M}} \right) (\varphi_0 - \varphi), \quad (\text{Eq S1}')$$

$$\nabla_{\perp}^2 \mathbf{u}_n + \nabla_{\perp} m - \left(\frac{KL^2}{\eta} \right) \varphi \nabla_{\perp} p = \left(\frac{KL^2}{\eta} \right) (\mathbf{u}_n - \mathbf{u}_s) + \left(\frac{\xi L^2}{\eta} \right) \mathbf{u}_n, \quad (\text{Eq S2}')$$

$$(1-\varphi) \nabla_{\perp} p = (\mathbf{u}_n - \mathbf{u}_s), \quad (\text{Eq S3}')$$

$$\frac{\partial m}{\partial t} = \left(\frac{D\eta}{\sigma\bar{M}L^2} \right) \nabla_{\perp}^2 m - \nabla_{\perp} \cdot (\mathbf{u}_n m), \quad (\text{Eq S4}')$$

$$\nabla_{\perp}^2 h = \left(\frac{\sigma K \bar{M} L^3}{\eta \varepsilon \gamma} \right) p \text{ at } z = h(x, y, t). \quad (\text{Eq S5'})$$

Importantly, the system of equation becomes 2D in the thin-cell approximation, justifying the widely use 2D approximation for flat dynamic lamellipodia. As equation (Eq S5') demonstrates, this approximation is valid in the limit of the high membrane tension, when non-dimensional combination of parameters $(\sigma K \bar{M} L^3 / \eta \varepsilon \gamma)$ is on the order of unity or smaller, $\gamma \sim (\sigma K \bar{M} L^3 / \eta \varepsilon)$. Mathematically, this means that the membrane tension has to be high enough so that parameter $\varepsilon \sim (\sigma K \bar{M} L^3 / \eta \gamma) \ll 1$. Physically, this means that if the membrane tension is high enough, it flattens the dorsal cell surface against the hydrostatic pressure of the cytosol. In fact, more relaxed inequality leads to a 2D class of models (Oliver et al., 2005), but here we wish to avoid complex derivations.

The validity of the 2D approximation is further supported by the observations of lamellipodial fragments that do not have a cell body. Their motility properties are very similar to those of the whole cell (Ofer et al., 2011). The fragments are extremely flat; even in their rear part, which is thicker than the front, they are only about one micron-thick, an order of magnitude less than their length and width (Ofer et al., 2011). There are many suggestions that the lamellipodium is the autonomous mechanical engine of the cell, while the 3D cell body simply rides passively atop of the lamellipodial actomyosin mesh (Rafelski and Theriot, 2004), but even taking the cell body into account does not change the thin-cell approximation, as the cell body thickness is but a few microns. Thus, the essential mechanics of the cell crawling on flat 2D surfaces is described well by the 2D model.

Furthermore, Rubinstein et al. (2009) estimated that Darcy friction between the cytosol and porous cytoskeletal network is roughly an order of magnitude smaller than effective viscous deformation forces within the cytoskeletal network:

$KL^2 / \eta \ll 1$. This strong inequality leads to the significant simplification of the model. Indeed, as small terms $\left(\frac{KL^2}{\eta} \right) \phi \nabla_{\perp} p$ and $\left(\frac{KL^2}{\eta} \right) (\mathbf{u}_n - \mathbf{u}_s)$ can be neglected in equation (Eq S2') compared

to the other terms of the order of unity in this equation (pressure and Darcy friction are weaker than the effective viscous deformation, adhesion and myosin contraction forces), the equations for the network mechanics can be uncoupled from the equations for the cytosol: approximate equations

$$\nabla_{\perp}^2 \mathbf{u}_n + \nabla_{\perp} m = \left(\frac{\xi L^2}{\eta} \right) \mathbf{u}_n, \quad (\text{Eq S1''})$$

$$\frac{\partial m}{\partial t} = \left(\frac{D\eta}{\sigma \bar{M} L^2} \right) \nabla_{\perp}^2 m - \nabla_{\perp} \cdot (\mathbf{u}_n m), \quad (\text{Eq S2''})$$

can be solved independently from the equations for the cytosol:

$$\frac{\partial \phi}{\partial t} + \nabla_{\perp} \cdot (\phi \mathbf{u}_n) = \left(\frac{r\eta}{\sigma \bar{M}} \right) (\phi_0 - \phi), \quad \frac{\partial (1-\phi)}{\partial t} + \nabla_{\perp} \cdot ((1-\phi) \mathbf{u}_s) = - \left(\frac{r\eta}{\sigma \bar{M}} \right) (\phi_0 - \phi), \quad (\text{Eq S3''})$$

$$(1-\varphi)\nabla_{\perp}p = (\mathbf{u}_n - \mathbf{u}_s), \quad (\text{Eq S4''})$$

$$\nabla_{\perp}^2 h = \left(\frac{\sigma K \bar{M} L^3}{\eta \varepsilon \gamma} \right) p \text{ at } z = h(x, y, t). \quad (\text{Eq S5''})$$

Note that if one wants information about the volume fraction, pressure and cytosol flow, one needs to solve Eqs (S3''-5'') together with Eqs (S1''-2''). However, Eqs (S1''-2'') are self-consistent: there is no need to know pressure or actin volume fraction to find the myosin and network flow distributions. Eqs (S1''-2'') constitute the 2D model in the main text that we use. This argument supports the idea that there exists the experimentally relevant limiting case, in which the full 3D model is reduced to the 2D model, in which the pressure can be neglected.

Lastly, let us note that we did not discuss the very difficult problem of the boundary condition at the contact line – intersection of the dorsal and ventral surfaces. Respective physics is not well understood, and majority of existent 2D models use the free boundary conditions similar to that used in our model here (Oliver et al., 2005).

Adding actin dynamics to the model.

There could be, of course, a pressure term in an equation for a compressible medium as well. In order to do consider effects of such term, as well as consequences of possible density dependence of the actin viscosity, we explicitly introduced dynamic actin densities into the ZS model. Dynamics of actin density are governed by a combination of the F-actin disassembly and drift with the same velocity, as that in the equation for myosin. To consider the actin dynamics quantitatively, we added the following equation for the actin density, F , to the model equations for the ZS model described in the main text:

$$\partial_T F = -\nabla \cdot (\mathbf{U}F) - k_{dis} F \quad (\text{Eq S6})$$

on $\Omega(t)$. The boundary condition we used was: $F|_{\partial\Omega(t)} = F_0$. The equation for the velocity (force-balance equation) changed as follows:

$$\eta \nabla \cdot \left(\left(1 + \frac{\varepsilon F}{F_0} \right) \nabla \mathbf{U} \right) + \sigma \nabla \cdot (\mathbf{M}\hat{I}) - \zeta \nabla \cdot (\mathbf{F}\hat{I}) - \xi \mathbf{U} = 0 \quad (\text{Eq S7})$$

With respective change in the boundary condition:

$$\mathbf{n} \cdot \left(\eta \left(1 + \frac{\varepsilon F}{F_0} \right) \nabla \mathbf{U} + \sigma \mathbf{M}\hat{I} - \zeta \mathbf{F}\hat{I} \right) |_{\partial\Omega(t)} = 0 \quad (\text{Eq S8})$$

To investigate implications of such actin dynamics, we accounted for the dependence of actin

viscosity on actin density (reflected in the factor $\left(1 + \frac{\varepsilon F}{F_0} \right)$, assumed to be proportional to the

actin density) and the effective swelling pressure (reflected in the term $\zeta \mathbf{F}\hat{I}$, also assumed to be proportional to the actin density). We found that the model worked well with simple protrusion

rate of the form: $V_p = V_0 \frac{A_0}{|\Omega|} - K |\Omega|$. We simulated the model using the non-dimensional

parameter values $v_0 = 1$, $\mu_{tot} = 1.5708$, $\alpha = 0.5$, for which the ZS model without actin predicted the cell moving straight. We found that as with our original model, the expanded model with explicit actin densities has stationary, translating, and rotating steady states. Namely, for small values of the swelling pressure ($\varepsilon = 0.01$, $k_{dis} = 1$, $\zeta = 0.5$), the simulated cell moved straight and steadily. For greater values of the swelling pressure ($\varepsilon = 0.01$, $k_{dis} = 1$, $\zeta = 1$), the simulated cell remained stationary and symmetric. This is easy to understand because the swelling pressure effectively counteracts the myosin contractile stress. If, on the other hand, we increase the protrusion rate (in the simulations we did that by changing the protrusion rate to $V_p = V_0 \frac{A_0}{|\Omega|} - K(|\Omega| - A_0)$, or effectively adding the term KA_0 to the protrusion rate), we expect the rotating cell, which indeed was the case ($\varepsilon = 0.01$, $k_{dis} = 1$, $\zeta = 0.14$).

Note on the anti-crowding terms in the model equations.

It is possible that the anti-crowding effects come from an attenuation of the myosin stress when the myosin density is too high. To explore this possibility, the factor $(1 - M/M_{tot})$ was removed from the advection term of the equation for myosin and inserted into the active stress term of the equation for velocity: $\nabla \cdot (M \left(1 - \frac{M}{M_{max}}\right) \mathbf{I})$, with the same M_{max} that was previously used in the advection term (the ‘anti-crowding’ term for diffusion was either kept as before, or removed in that case, with no significant effect on the results). Simulations were run for three cases depicted in Fig. 1, and the results were compared against the original results for several metrics as summarized in three tables below:

ZS: Stationary cell ($\mathbf{v}_0, \mu_{tot}, \alpha$) = (2.5, 0.125 π , 0.5)

Measured parameter	Nonlinear advection $\nabla \cdot (\mathbf{v} \left(1 - \frac{M}{M_{max}}\right) \mathbf{M})$	Nonlinear contractility $\nabla \cdot (M \left(1 - \frac{M}{M_{max}}\right) \mathbf{I})$
Aspect ratio	1.00	1.00
Steady-state area of the cell	3.49	3.50
max(Myosin) at steady-state	0.13	0.13
min(Myosin) at steady-state	0.09	0.09

ZV: Translating cell ($\mathbf{v}_0, \mu_{tot}, \alpha$) = (2.5, 2 π , 0.5)

Measured parameter	Nonlinear advection $\nabla \cdot (\mathbf{v} \left(1 - \frac{M}{M_{max}}\right) \mathbf{M})$	Nonlinear contractility $\nabla \cdot (M \left(1 - \frac{M}{M_{max}}\right) \mathbf{I})$
Translational cell speed	0.19	0.18
Aspect ratio	1.63	1.33
Steady-state area of the cell	3.85	3.84
max(Myosin) at steady-state	13.96	11.35
min(Myosin) at steady-state	0.01	0.05

ZS: Rotating cell ($\mathbf{v}_0, \mu_{tot}, \alpha$) = (2.5, 0.75 π , 0.5)

Measured parameter	Nonlinear advection $\nabla \cdot (\mathbf{v} \left(1 - \frac{M}{M_{\max}}\right) \mathbf{M})$	Nonlinear contractility $\nabla \cdot (\mathbf{M} \left(1 - \frac{M}{M_{\max}}\right) \mathbf{I})$
angular velocity	0.58	0.37
Radius of rotation	1.12	1.11
Aspect ratio	2.13	1.71
Steady-state area of the cell	2.74	2.86
max(Myosin) at steady-state	9.22	5.35
min(Myosin) at steady-state	0.01	0.03

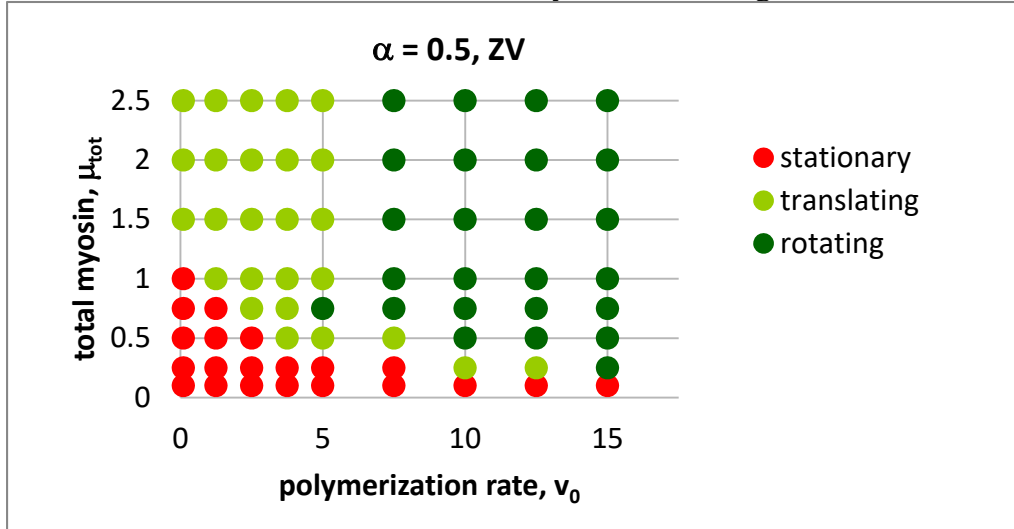
The results indicated that the stationary, rotational, and unidirectional behaviors are qualitatively the same as in our original models, and even quantitative characteristics of the solutions are close to the original. Of course, the boundaries between the corresponding regions in the state diagrams change, but only a little.

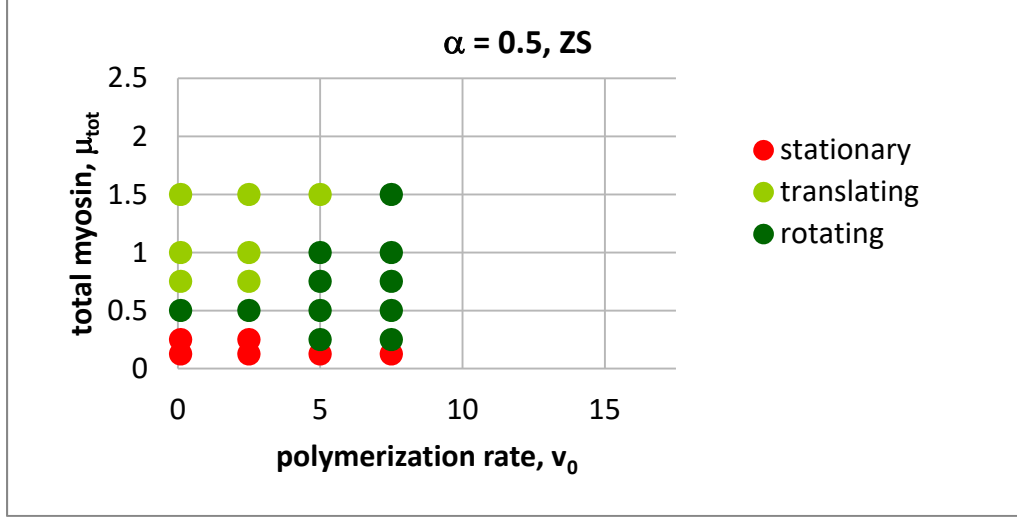
Derivations and assumptions related to the protrusion rates.

We originally used different expressions for the boundary protrusion rate V_p in the two models for the following reason. The dependence of V_p on myosin is essential in the ZV model, as has been discussed in detail in the main text: without it, the cell never moves and changes shape in this version of the model. In the ZS model, the cell moves and changes shape with V_p independent of myosin, and so we decided to test this simplest case. The usage of different exponents ($n=0$ in ZV and $n=2$ in ZS) was due to the fact that we initially wanted to find the smallest integer exponent n for which the model predicted a stable behavior. It turned out that $n=0$ was the smallest for the ZV model, and $n=2$ for the ZS model. By using a myosin-dependent V_p in the ZS model and increasing n to $n=2$ in the ZV model, one can unify the models, simplify the number of choices, and also demonstrate robustness of the models. So we explored the models with the same protrusion velocity,

$$V_p = V_0 \left(\frac{A_0}{A} \right) \left(1 + \frac{M|\partial\Omega(\mathbf{v})|}{M_0} \right)^{-1} - K(A - A_0 \left(\frac{A_0}{A} \right)^2). \quad (\text{Eq S9})$$

We found that this resulted in an essentially same state diagram for the ZV model:





The state diagram of the ZS model also remains qualitatively similar to that in the main text, with the following differences: i) the border between the stationary and moving states is now slightly dependent on M , like in our ZV diagram; ii) the region of rotating states has shrunk somewhat; 3) cells move faster due to the enhanced coupling between front velocities and myosin.

Biophysics underlying the expression for the protrusion rate V_p is based on the force balance at the lamellipodial boundary. As the lamellipodium is essentially flat, the force balance at this boundary is quite simple: There is an outward polymerization force exerted by growing actin filament tips abutting the plasma membrane, F_{pol} , complemented by the effective elastic resistance of the actin cortex and the cell body, F_{res} , balanced by the inward membrane tension, T (all forces are per micron of the cell edge.) Thus,

$$F_{pol} + F_{res} = T \quad (\text{Eq S10})$$

It was shown that membrane bending forces are negligible compared to the effect of the membrane tension (Kozlov and Mogilner, 2007). We also assume that adhesion between the actin network and plasma membrane can be neglected.

The polymerization force is proportional to the density of growing actin filaments per unit length of the cell edge, N . As was noted in our supplemental material, we assume that the actin tip density at the boundary depends on the cell area (Lieber et al., 2013) because of a limited amount of actin regulatory proteins; specifically, we assume that this density is inversely proportional to the lamellipodial area: $N = N_0 / A$, where A is the lamellipodial area and N_0 is the proportionality coefficient. Furthermore, the polymerization force is a decreasing function of the protrusion rate. In the limited range of the protrusion rates, this dependency can be approximated with the linear function:

$$F_{pol} = NF_p - \mathcal{G}V_p, N = \frac{N_0}{A} \quad (\text{Eq S11})$$

where \mathcal{G} is the proportionality coefficient and F_p is the stall force per filament.

The membrane tension is spatially uniform, and it is an increasing function of the lamellipodial area (Lieber et al., 2013). Mechanically, this is likely due to the fact that the increase of the lamellipodial area, while the total plasma membrane area remains constant on the relevant time scale, makes the membrane flatter in the cell body region, thus squeezing the viscoelastic cell body and creating the mechanical tension. In our model, we assume that the membrane tension is proportional to the lamellipodial area: $T \sim A$. The mechanical effect from the elastic resistance of actin cortex and the cell body that counters too much shrinking of the cell area has to increase sharply with the decrease of the lamellipodial area. We assume that respective resistance force is inversely proportional to the n^{th} degree of the lamellipodial area: $F_{res} \sim A^{-n}$. We define the characteristic cell area A_0 as the area at which the opposing membrane tension and elastic cell body resistance forces are balanced: $T = F_0 (A / A_0) = F_0 (A_0 / A)^n = F_{res}$. Here F_0 is this balanced force magnitude at the characteristic cell area. Thus:

$$T = F_0 (A / A_0) \quad (\text{Eq S12})$$

$$F_{res} = F_0 (A_0 / A)^n \quad (\text{Eq S13})$$

By substituting Eqs (S11-13) into Eq (S10), we arrive at the expression for the protrusion rate in the ZS model:

$$V_p = V_0 (A_0 / A) - K (A - A_0 (A_0 / A)^n) \quad (\text{Eq S14})$$

$$\text{where } V_0 = \frac{N_0 F_p}{\mathcal{G} A_0}, K = \frac{F_0}{\mathcal{G} A_0}.$$

As we wrote above, the protrusion rate has to be an increasing function of the local actin density. In some special cases, the actin density and the protrusion rate are, in fact, almost uniform around the cell boundary: this was the reported case for keratocytes moving on weakly adhesive surfaces (Barnhart et al., 2011). Thus, we made the respective simplest assumption for the ZS model.

The expression for the protrusion rate in the ZV model is based on a similar force balance. In the ZV model, the nontrivial solutions require a non-uniform rate of protrusion. In majority of cases, indeed, the rate of protrusion is maximal at the leading edge and decreases to the sides and rear of the cell (Barnhart et al., 2011). Coincidentally, myosin density increases towards the rear of the motile cell. A recent study (Lomakin et al., 2015) strongly suggests that myosin contraction locally destroys the protrusive branched actin network, and so the branched actin density and protrusion rate are decreasing function of the local myosin density. This is reflected by the term $V_p A_0 / (A(1+M/M_0))$.

Notes on the myosin transport.

The assumption behind the myosin transport equation in our model is that myosin binding kinetics are fast compared to the transport terms and, are therefore, rapidly equilibrated. In that case, two equations for two sub-populations of myosin, one – myosin bound to actin network and drifting with the network, another – diffusing in the cytosol, have the form:

$$\begin{aligned}\partial_t m_b &= -\nabla \cdot (\mathbf{u} m_b) + k_{on} m_f - k_{off} m_b \\ \partial_t m_f &= \nabla \cdot (d \nabla m_f) - k_{on} m_f + k_{off} m_b\end{aligned}\tag{Eq S15}$$

When the kinetics is fast, $k_{on} m_f \approx k_{off} m_b$, and this system of equations reduces to the single equation for the total local myosin, $m = m_f + m_b$:

$$\partial_t m = \nabla \cdot (\bar{d} \nabla m_f - \bar{\mathbf{u}} m), \bar{d} = d \frac{k_{off}}{k_{on} + k_{off}}, \bar{\mathbf{u}} = \mathbf{u} \frac{k_{on}}{k_{on} + k_{off}}.\tag{Eq S16}$$

To make sure that the approximation is valid, we simulated the models with myosin transport equation (2) in the main text replaced by the system of equations (Eq S15), with $k_{on}, k_{off} \gg 1$.

Specifically, we simulated the model with myosin transport described by Eq S15, in three cases:

Model	Parameter set (v_0, μ_{tot}, α)	Mechanical state
ZS	(7.5, $\pi/4$, 1)	Stationary
ZS	(7.5, $\pi/2$, 1)	Rotating
ZV	(7.5, $\pi/2$, 1)	Translating

Results indicated that the model formulated in terms of two myosin sub-populations is essentially identical to the corresponding model described in the main text when $k_{on}, k_{off} \gg 1$.

Our models have common features with the one in (Wolgemuth et al., 2011). In the latter, steadily migrating solutions were not found. Out of 3 types of solutions found in (Wolgemuth et al., 2011), one – a stationary cell at low contractility – is the same as in our case. Another – when contractility is higher – created a cell ‘pinched’ into the dumbbell shape. We observed such shapes transiently, but they rapidly became rotating. The third solution corresponded to parameter α being very small, in which case of cell developed into a ‘sausage’-like shape. Our model with small α (~ 0.1) still exhibits steadily motile (straight and rotating) shapes.

We believe that these discrepancies are caused by the differences between our model and that in (Wolgemuth et al., 2011). One significant difference is that in the transport equation system of (Wolgemuth et al., 2011), Eq S15, the free myosin instantaneously levels off, implying the infinite diffusion coefficient. The fast diffusion assumption means that the time of dissipation of gradients of free myosin is much shorter than the time scale of the model defined as L/V_0 , i.e. $L^2/D \ll L/V_0$, or $V_0 L/D \ll 1$. In our models, $V_0 L/D = v_0$ is the dimensionless version of V_0 . Thus, if it were not for other differences with our models, the model of (Wolgemuth et al., 2011) would be equivalent to the limit of slow protrusion in our models. In this limit, the ZV model has only stationary solutions, even for asymmetric myosin, and the ZS model does not have rotational solutions for $\alpha = 1$. There is another difference caused by the finiteness of diffusion in our models, which likely explains why the unidirectional (and rotational, for $\alpha = 0.5$) motility in the ZS model for small v_0 was not observed in the model of (Wolgemuth et al., 2011). Because the diffusion coefficient is finite in our models, we account for volume excluded by myosin to avoid the singularities, which apparently do not occur if the diffusion is infinitely fast. As a result, the bound myosin does not form tight, delta-function-like aggregates for intermediate values of myosin, making the cell boundary more dynamic. Finally, there are minor differences

in the expressions for the boundary protrusion velocity used in our study and (Wolgemuth et al., 2011).

Barnhart EL, Lee KC, Keren K, Mogilner A, Theriot JA. An adhesion-dependent switch between mechanisms that determine motile cell shape. *PLoS Biol.* 2011 9:e1001059.

Cogan NG, Guy RD. 2010. Multiphase flow models of biogels from crawling cells to bacterial biofilms. *HFSP J.* 4(1):11—25

Dembo M, Harlow F. 1986. Cell motion, contractile networks, and the physics of interpenetrating reactive flow. *Biophys. J.* 50(1):109--21

Drew DA, Segel LA. 1971. Averaged equations for two-phase flows. *Stud. Appl. Math.* 50(3):205--31

Kozlov MM, Mogilner A. Model of polarization and bistability of cell fragments. *Biophys J.* 2007 Dec 1;93(11):3811-9.

Kuusela E, Alt W. 2009. Continuum model of cell adhesion and migration. *J. Math. Biol.* 58(1--2):135--61

Lieber AD, Yehudai-Resheff S, Barnhart EL, Theriot JA, Keren K. Membrane tension in rapidly moving cells is determined by cytoskeletal forces. *Curr Biol.* 2013 23:1409-17.

Lomakin AJ, Lee KC, Han SJ, Bui DA, Davidson M, Mogilner A, Danuser G. Competition for actin between two distinct F-actin networks defines a bistable switch for cell polarization. *Nat Cell Biol.* 2015 17:1435-45.

Ofer N, Mogilner A, Keren K. Actin disassembly clock determines shape and speed of lamellipodial fragments. *Proc Natl Acad Sci U S A.* 2011 108:20394-9.

Oliver JM, King JR, McKinlay KJ, Brown PD, Grant DM, et al. 2005. Thin-film theories for two-phase reactive flow models of active cell motion. *Math. Med. Biol.* 22(1):53—59

Rafelski SM, Theriot JA. Crawling toward a unified model of cell mobility: spatial and temporal regulation of actin dynamics. *Annu Rev Biochem.* 2004 73:209-39.

Rubinstein B, Fournier MF, Jacobson K, Verkhovsky AB, Mogilner A. Actin-myosin viscoelastic flow in the keratocyte lamellipod. *Biophys J.* 2009 97:1853-63.

Wolgemuth CW, Stajic J, Mogilner A. Redundant mechanisms for stable cell locomotion revealed by minimal models. *Biophys J.* 2011 101:545-53.